Review

Heavy-Flavour Jets in High-Energy Nuclear Collisions

Sa Wang, Wei Dai, Enke Wang, Xin-Nian Wang and Ben-Wei Zhang

MDPI

Review

Heavy-Flavour Jets in High-Energy Nuclear Collisions

Sa Wang [1,2] (ORCID), **Wei Dai** [3], **Enke Wang** [1,2], **Xin-Nian Wang** [4] and **Ben-Wei Zhang** [1,2,*]

1   Guangdong Provincial Key Laboratory of Nuclear Science, Institute of Quantum Matter,
     South China Normal University, Guangzhou 510006, China
2   Key Laboratory of Quark & Lepton Physics (MOE) and Institute of Particle Physics,
     Central China Normal University, Wuhan 430079, China
3   School of Mathematics and Physics, China University of Geosciences, Wuhan 430074, China
4   Nuclear Science Division MS 70R0319, Lawrence Berkeley National Laboratory, Berkeley, CA 94720, USA
*   Correspondence: bwzhang@mail.ccnu.edu.cn

Abstract: Reconstructed jets initiated from heavy quarks provide a powerful tool to probe the properties of the quark–gluon plasma (QGP) and to explore the mass hierarchy of jet quenching. In this article, we review the recent theoretical progresses on heavy-flavour jets in high-energy nuclear collisions at the RHIC and LHC. We focus on the yields and substructures of charm and bottom quark jets with jet-quenching effects, such as the nuclear modification factors, transverse momentum imbalance, angular correlation, radial profiles, fragmentation functions, the "dead-cone" effect, etc.

1. Introduction

High-energy nuclear collisions at the Relativistic Heavy Ion Collider (RHIC) and Large Hadron Collider (LHC) have opened up new avenues for the search for strongly interacting nuclear matter, the quark–gluon plasma (QGP) [1–4]. Investigating the formation of the QGP deepens our understanding of quantum chromodynamics (QCD) under extreme conditions at high temperature and density [5,6] and the evolution of the Universe at the first microsecond [7]. The jet-quenching phenomena, the energy attenuation of fast partons due to their strong interactions with the QCD medium, provide an army of powerful tools to study the properties of the QGP, such as the yield suppression of high-p_T hadron/jet, the p_T asymmetry of dijets, γ/Z^0+ jets as well as jet substructures [8–21].

In elementary proton–proton reactions, the productions of charm and bottom quarks are perturbatively calculable, since their large masses ($M_c \sim 1.5$ GeV, $M_b \sim 4.8$ GeV) act as a natural cut-off above the Λ_{QCD} [22]. Heavy quarks are produced in the initial hard scattering at a very early stage due to their large masses, therefore witnessing the whole QGP evolution. Meanwhile, while their thermal production is almost negligible with the initial conditions so far accessible in heavy-ion programs at the RHIC and LHC [23], the productions of charm and bottom hadron/jets make a very promising hard probe to the transport properties of hot and dense quark matter. During the past decade, the experimental measurements including the nuclear modification factor R_{AA} [24–30] and the collective flow (the direct flow v_1 [31,32] and elliptical flow v_2 [33–36]) of heavy-flavour hadrons both at the RHIC and LHC have attracted much attention from the community of high-energy nuclear physics.

A lot of theoretical studies have been performed to confront the experimental data obtained in the high-energy heavy-ion collisions, which greatly improve our understanding of the in-medium evolution [37–58] and hadronization mechanisms [59–61] of heavy quarks (for detailed reviews see [62–70]). Specifically, the current models treat the elastic and inelastic interactions between heavy quarks and the QGP medium with multiple methods, consisting mainly the perturbative or non-perturbative analytic calculations (SCET [41,71], CUJET [46,72], DREENA [73–78], WHDG [79,80], AdS/CFT (HG) [81,82]), and the Monte

Carlo transport approaches based on the Boltzmann (BAMPS [83–86], MC@$_s$HQ [87–89], (Q)LBT [47,57], LIDO [49,90], Catania-pQCD/QPM [91–94]), the Langevin (POWL ANG [45,95,96], Duke [44,97], UrQMD [98–100], TAMU [40,101,102], SHELL [103–105]) and the Kadanoff–Baym (PHSD [106–108]) equations. These phenomenological studies reveal a fact that the elastic scattering of heavy quarks in the hot/dense nuclear matter is important, especially at the lower p_T region ($p_T^Q < 5m_Q$), different from our experience of treating light quarks or gluons. One of the central issues of investigating the heavy-flavour production in the heavy-ion program is extracting the diffusion coefficient D_s, which is directly related to the transport properties of the hot QCD matter. Additionally, different from the fragmentation hadronization of heavy quarks in a vacuum, within the hot and dense nuclear matter, the heavy-flavour hadrons can be produced by a combination of heavy quarks and thermal partons. Such a coalescence hadronization mechanism plays an important role in the collective flow [33,34] and baryon-to-meson ratio [109,110] of charmed hadron in nucleus–nucleus collisions at the RHIC and LHC.

In recent years, the experimental measurements on heavy-flavour jet (a reconstructed jet containing a heavy quark or a heavy-flavour hadron) have made great strides in p+p [111–118], p+A [111,119,120] and A+A collisions [121–128]. A wealth of information carried by heavy-flavour jets not only offers a new topic of jet physics and the application of the perturbative QCD, but also their medium modifications in heavy-ion collisions are also of great significance to reveal the in-medium energy loss mechanism of heavy quarks, to address the mass effect of jet quenching, and to extract the transport properties of the QGP.

2. Recent Advances of Heavy-Flavour Phenomenology in Heavy-Ion Collisions

Generally speaking, as we discussed in the last section, the reason for treating the heavy flavours as powerful hard probes to the transport properties of the QGP consists of at least three aspects. Firstly, the large mass ($M_Q \gg \Lambda_{QCD}$) makes it available to compute the differential cross-section of heavy quarks in the binary nucleon–nucleon collisions based on the perturbative QCD (pQCD) scheme within the next-to-next-to-leading order (NNLO) precision [129]. Secondly, due to the large mass ($M_Q \gg T_{med}$), the total yield of heavy quarks in nucleus–nucleus collisions only depends on their initial production at hard scattering. Since the momentum transfer of the in-medium collisions $q^2 \sim g^2T^2$ ($T \sim 0.4$–0.5 GeV) is much smaller than the creation energy of heavy quark pairs at the current collision energy, both at the RHIC and LHC, the subsequent contribution from the thermal creation during the QGP evolution is negligible [23]. Apart from this, according to the Heisenberg uncertainty principle, the formation time of heavy quarks ($\tau_0 \sim \frac{1}{2m_Q} < 0.1$ fm/c) is shorter than the formation time of the quark–gluon plasma ($\tau_f \sim 0.6$ fm/c). Therefore heavy quarks witness the entire evolution of the hot/dense nuclear matter until the freeze-out. In this section, we will briefly introduce the recent theoretical advances that help us understand the heavy-flavour production in heavy-ion collisions, including mainly the following several aspects, the initial production, the transport approaches, the hadronization mechanisms, and the extraction of diffusion coefficient.

2.1. Production of Heavy Quarks in p+p Collisions

The production of heavy quarks in proton–proton collisions establishes a baseline to investigate the nuclear modification in high-energy nuclear collisions both at the RHIC and LHC. The yield of heavy flavours in nucleus–nucleus collisions generally is viewed as the sum of that in N_{coll} binary nucleon–nucleon collisions while taking into account the initial cold nuclear matter effect (usually considered by using the nuclear-modified parton distribution function [130–132]). In the fixed-flavour-number scheme (FFNS) [22], the cross-section of heavy quarks in p+p collisions can be expressed based on the factorization theorem,

$$d\sigma_Q[s, p_T, y, m_Q] \simeq \sum_{i,j} \int_0^1 dx_i \int_0^1 dx_j f_i^A(x_i, \mu_F) f_j^A(x_j, \mu_F) d\tilde{\sigma}_{ij \to Q+X}[x_i, x_j, s, p_T, y, m_Q, \mu_F, \mu_R] \tag{1}$$

where s is the square of the centre-of-mass energy of the incoming proton, p_T is the transverse momentum of the produced heavy quark, and y is the rapidity. f_i^A (f_j^B) is the parton distribution function (PDF) quantifying the probability to find a parton with flavour $i(j)$ and carrying momentum fraction $x_{i(j)}$ in the colliding proton $A(B)$, which relies on the factorization scale μ_F. $\tilde{\sigma}_{ij \to Q+X}$ represents the cross-section of the partonic hard process $i + j \to Q + X$ that can be calculated relying on the pQCD. The partonic cross-section $\tilde{\sigma}_{ij \to Q+X}$ also relies on the strong coupling constant α_s determined at the renormalization scale μ_R. Note that Equation (1) sums all partonic hard processes $i + j \to Q + X$, where i, j are the active flavours including $(u, \bar{u}, d, \bar{d}, s, \bar{s}, g)$ but not heavy quarks. Only at the factorization scale $\mu_F > m_c$, can charm be viewed as an active flavour, often used for beauty production. The differential cross-section $d\sigma_Q$ can be convolved with a scale-independent fragmentation function $D_Q^H(z)$, such as the Peterson [133] or Lund [134] forms, to obtain the cross-section of the heavy-flavour hadron,

$$d\sigma_H = d\sigma_Q \otimes D_Q^H(z) \tag{2}$$

where H denotes the heavy-flavour hadron and z the momentum fraction carried by H.

Since the FFNS is usually applicable at the low p_T region ($0 < p_T < 5m_Q$), for the higher kinematic region ($p_T \gg m_Q$), the logarithmic terms ($\frac{\alpha_s}{2\pi} ln(p_T^2/m_Q^2)$) in the perturbative expansion of the cross-section become large, and should be resummed to all orders. To implement such a resummation, one has to absorb the large logarithmic terms into the parton distribution function and fragmentation function. This treatment requires that heavy quarks are active flavours when the factorization scale is $\mu_F > m_Q$. In other words, such a scheme has a variable number of active flavours when μ_F crosses the heavy quark mass, hence named the variable-flavour-number scheme (VFNS). In particular, when the heavy quark mass can be neglected in the evaluation of the short-distance cross-section, the VFNS scheme is called the zero-mass VFNS (ZM-VFNS). In the ZM-VFNS, the differential cross-section of a heavy-flavour hadron based on the factorization theorem can be expressed as:

$$d\sigma_{H+X} \simeq \sum_{i,j} \int_0^1 dx_i \int_0^1 dx_j f_i^A(x_i, \mu_F) f_j^A(x_j, \mu_F) d\tilde{\sigma}_{ij \to k+X} D_k^H(z, \mu_F') \tag{3}$$

where $D_k^H(z, \mu_F')$ is given by a convolution of a perturbative-fragmentation function (PFF) $D_k^Q(z, \mu_F')$ describing a parton k fragmentation into heavy quark Q, with a scale-independent one $D_Q^H(z)$ for the hadronization of a heavy quark. Note that in Equation (3) the sum covers all possible partonic-hard processes ($i + j \to k + X$) where i, j, k can be light quarks, gluons, and heavy quarks [135]. Since heavy quark mass is neglected in the computation of the cross-section, the ZM-VFNS is expected to be reliable only at very high p_T.

To find a unified theoretical framework that combines the advantages of the FFNS at low p_T and the ZM-VFNS at high p_T, in recent years the interpolation schemes have been established, such as the general-mass VFNS (GM-VFNS) [136,137] and the fixed-order plus next-to-leading logarithms (FONLL) [129,138]. For instance, by using an interpolating function $G(m_Q, p_T) = p_T^2/(p_T^2 + c^2 m_Q^2)$ where c is set to $c = 5$, the FONLL scheme can well describe the heavy-flavour production in the entire kinematic region. For more details of the interpolation schemes see [22] and the references therein.

Compared to the analytic calculation schemes discussed above, the general-purpose Monte Carlo event generator, such as PYTHIA [139], HERWIG [140], POWHEG [141] and SHERPA [142], can provide a more complete description of all the final-state particles at the parton or hadron level. Especially for the studies of jet physics, the Monte Carlo event generators can give more precise descriptions of the observations relating to the jet substructure than analytic calculations.

2.2. Transport of Heavy Quarks in the QGP

Transport approaches are wildly used in the current theoretical studies of heavy-flavour production in high-energy nuclear collisions. At the lower p_T region, the elastic scattering of heavy quarks with the thermal parton (light quark or gluon) has been proven to be the dominant mechanism of energy loss. Generally, the kinetic theory based on the Boltzmann transport equation is a popular treatment for in-medium heavy quark evolution. The Boltzmann equation for the distribution function of heavy quarks can be written in a compact form,

$$p_\mu \partial_\mu f_Q(x, p) = C[f_q, f_{\bar{q}}, f_g, f_Q](x, p) \tag{4}$$

where $f_Q(x, p)$ is the phase-space distribution of heavy quarks. In the QGP, the phase-space distributions of light quark f_q and gluon f_g can be solved by the Boltzmann equation [143,144]. Subsequently, the relativistic Boltzmann-like collision integral $C[f_Q](x, p)$ has a simplified form [42,145],

$$C[f_Q] = \int d^3q[\omega(\mathbf{p} + \mathbf{q}, \mathbf{q})f_Q(\mathbf{x}, \mathbf{p} + \mathbf{q}, t) - \omega(\mathbf{p}, \mathbf{q})f_Q(\mathbf{x}, \mathbf{p}, t)] \tag{5}$$

where $\omega(\mathbf{p} + \mathbf{q}, \mathbf{q})$ represents the transition rate of a heavy quark from the momentum $\mathbf{p} + \mathbf{q}$ to $\mathbf{p}$ by collisions with quasiparticles. This rate is usually determined by the matrix elements of the $2 \to 2$ QCD scattering. With the assumption that the momentum transfer $|\mathbf{q}|$ is small compared to the momentum of a heavy quark, we can expand $\omega(\mathbf{p} + \mathbf{q}, \mathbf{q})f_Q(\mathbf{x}, \mathbf{p} + \mathbf{q}, t)$ around $\mathbf{q}$ by utilizing the Taylor formula to obtain the Fokker–Planck equation,

$$\frac{\partial f_Q}{\partial t} = \frac{\partial}{\partial p_i}\left[A_i(\mathbf{p})f_Q + \frac{\partial}{\partial p_j}[B_{ij}(\mathbf{p})f_Q]\right] \tag{6}$$

where two coefficients $A_i(\mathbf{p}) = \int d^3q\omega(\mathbf{p}, \mathbf{q})q_i$ and $B_{ij}(\mathbf{p}) = \int d^3q\omega(\mathbf{p}, \mathbf{q})q_iq_j$ are directly related to the drag coefficient (η_D) and the momentum diffusion coefficient (κ), which control rate of the energy loss and the momentum broadening of heavy quarks in the hot medium, respectively. Indeed, the Fokker–Planck equation is equivalent to another more well-known equation, the Langevin equation,

$$\frac{d\vec{x}}{dt} = \frac{\vec{p}}{E} \tag{7}$$

$$\frac{d\vec{p}}{dt} = -\eta_D(p)\vec{p} + \vec{\xi}(t) \tag{8}$$

where the stochastic term $\vec{\xi}(t)$ describes the random kicks suffered in heavy quarks from the medium constituents, which obeys a Gaussian distribution with a mean value 0 and variance κ. The drag coefficient η_D and the diffusion coefficient κ are related by the fluctuation–dissipation theorem (FDT) $\kappa = 2\eta_D ET$. Note that at higher kinematic regions ($p_T^Q > 5m_Q$), the medium-induced gluon radiation plays an increasingly important role in the energy loss of heavy quarks. The radiative energy loss of heavy quarks is treated with various formalisms and at different approximations [53,146–150], which usually provide the radiated gluon spectra as a function of momentum fraction x and transverse momentum $k_\perp$. In the Langevin equation, the radiative energy loss of heavy quarks can be coupled with the collisional one by adding a recoil term $-\vec{p}_g$ caused by the radiated gluon [44]. The four-momentum of the radiated gluon can be easily sampled based on the radiation spectra $dN_g/dxdk_\perp^2$.

In many of the recently developed theoretical frameworks modelling the production of heavy flavour in heavy-ion collisions, the Boltzmann and Langevin equations are the two most popular choices, especially for Monte Carlo simulations. Concerning the performance of these two approaches, detailed comparisons have been discussed in [151,152]. In

general, the implementation of the Boltzmann equation implies that the medium consists of well-defined quasiparticles, while the Fokker–Planck (Langevin) equation is realized in a more general way without the quasiparticle assumption. However, the advantage of the Boltzmann equation is that it can naturally describe the heavy quark evolution even under off-equilibrium conditions, which may be the case of the early pre-equilibrium stage in heavy-ion collisions [153].

2.3. Hadronization: Fragmentation and Coalescence

Studying the yield suppression and collective flow of heavy-flavour hadrons also deepens our understanding of heavy quark hadronization in nucleus–nucleus collisions, which shows different mechanisms with that in a vacuum. As discussed in Section 2.1, fragmentation functions describe the non-perturbative hadronization process of heavy quarks into heavy-flavour hadron in a vacuum. The most commonly used fragmentation function is the Peterson form [133],

$$D_{H/Q}(z) = \frac{N}{z[1 - \frac{1}{z} - \frac{\epsilon_Q}{1-z}]} \tag{9}$$

where z denotes the momentum fraction carried by the heavy hadron from the heavy quark in the fragmentation process ($0 < z < 1$), which implies that the heavy hadron must have smaller energy than the heavy quark. The only tunable parameter in Equation (9) is ϵ_Q that can be determined by fitting to the measured spectra of the heavy-flavour hadrons. N is the normalization factor to guarantee $\int_0^1 dz D_{H/Q}(z) = 1$.

Measurements on the collective flow [33,34] and baryon-to-meson ratio [109,110] of charmed hadron A+A collisions suggest the existence of a new hadronization mechanism, coalescent of heavy quarks. The basic idea behind the coalescence mechanism is that a heavy quark can combine with a light anti-quark from the medium when they have enough small distance in the coordinate-momentum space. It means that the heavy-flavour meson has larger energy than the parent heavy quark, differing from the mechanism of fragmentation. The distribution function of the formed heavy-flavour meson usually can be obtained by a convolution with the following schematic form.

$$f_M \sim g_M f_{Q(\bar{Q})} \otimes f_{\bar{q}(q)} \otimes \phi_M \tag{10}$$

where g_M denotes the degeneracy of the heavy-flavour meson in spin and isospin, $f_{Q(\bar{Q})}$ and $f_{\bar{q}(q)}$ are the distribution functions of the heavy and light quarks in the coordinate-momentum space, respectively. ϕ_M represents the Wigner transform of the wave function of the heavy-flavour meson, commonly approximated by the ground state one of the simple harmonic oscillators [47].

In the realistic implementation of the heavy quark hadronization in nuclear collisions, the first step is to determine the probability of coalescence by integrating the distribution function of Equation (10). If coalescence occurs, one can sample a light anti-quark based on the thermal equilibrium distribution, otherwise Equation (9) is used to fragment the heavy quark into a hadron. At least in the lower p_T region, the experimental results favour the coalescence mechanism [94]. The coalescence of heavy quarks seems to decrease the suppression factor and enhance the collective flow of heavy-flavour hadrons, especially at $p_T < 6$ GeV. The recent studies [59,61] show that the coalescence mechanism is important in the description of the Λ_c/D^0 ratio measured by the STAR [109] and ALICE [110] collaborations. Additionally, the hadronic scattering between the D meson and light-flavour hadrons ($D - \pi$, $D - \rho$) has also been studied in [154], but its influence on the D meson R_{AA} was found to be very limited [155].

2.4. Extraction of the Diffusion Coefficient of Heavy Quarks

One of the most important goals of the heavy-ion collision experiment is to investigate the transport properties of the QCD matter under extremely hot and dense conditions.

As discussed above, due to the large mass ($m_Q \gg T_{\text{med}}$), heavy quarks are believed to be powerful tools for exploring the transport properties of the QGP. Phenomenological studies of heavy-flavour production in high-energy nuclear collisions provide a unique opportunity to extract the transport coefficient of the QGP, such as the momentum diffusion coefficient κ of heavy quarks, whose longitudinal and transverse components can be convenient to define as,

$$\kappa_{||} \equiv -\frac{d\left\langle (\Delta p_{||})^2 \right\rangle}{dt} \tag{11}$$

$$\kappa_\perp \equiv \frac{1}{2}\frac{d\left\langle (\Delta p_\perp)^2 \right\rangle}{dt} \tag{12}$$

where $\Delta p_{||}$ and $\Delta p_\perp$ momentum changes parallel and perpendicular to the heavy quark formulation. By definition, $\kappa_\perp$ can be directly related to the jet transport coefficient $\hat{q}$ which quantifies all the transverse momentum broadening of hard partons as traversing the QGP medium. Assuming that the κ is isotropic, namely, $\kappa_\perp = \kappa_{||} = \kappa$, one can obtain a simplified relation $\hat{q} = 2\kappa$. This relation has been employed in the modified Langevin equation to balance the two parts of the contribution from the collisional and radiative energy loss of heavy quarks [44,156]. Here we only overview the recent advances of the κ extraction by different model calculations. A more detailed and profound discussion about this topic can be found in [64].

The momentum diffusion coefficient κ can be easily converted to the spatial one D_s with the relation $\kappa = 2T^2/D_s$. In recent years, the temperature dependence of the dimensionless quantity $2\pi T D_s$ has been estimated by a lot of theoretical frameworks, such as the lattice QCD (lQCD) [157–159], LO pQCD [43,160], QPM calculations [92], T-matrix [40], PHSD [161], MC@$_s$HQ [22], Ads/CFT [162], duke (Bayesian analysis) [163], and hadronic matter [102,164], as shown in Figure 1.

The estimates by the lQCD from the first principles provide a valuable reference for the model extractions of $2\pi T D_s$. As one can see, with relatively large uncertainties, the lQCD calculations in the quenched approximation give $D_s \sim 3.7$–7.0 [159] over the temperature range from T_{pc} to $2T_{pc}$. However, it is difficult to extract meaningful information about the temperature dependence of $2\pi T D_s$ from the current lQCD results. Furthermore, except for the pQCD calculations at the leading-order which show obvious larger values than others, these extractions of $2\pi T D_s$ based on the recently developed models are consistent with the lQCD data, as well as previous studies presented in [64] which give $2\pi T D_s \sim 2$–4 near the critical temperature. Although these calculations give different values of $2\pi T D_s$ versus T/T_{pc}, most estimations show that D_s slightly increases with T. It implies that the interactions between a charm quark and the QCD medium have the strongest strength near the critical temperature. However, no direct evidence has been found in the experiment to verify this upward trend of D_s so far because it is hard to find an observation only sensitive to the in-medium interactions at the late stage of the QGP evolution. Fortunately, the data-driven analysis utilizing Bayesian inferences seems to shed new light on this issue. The temperature and momentum dependence of D_s has been extracted from the available experimental data (R_{AA} and v_2 of a D meson both at the RHIC and LHC) [163] based on the Duke–Langevin transport model, which indeed shows an upward trend of $2\pi T D_s$. More recently, this approach of Bayesian inference has been improved with the help of information field theory [165,166] in [167]. Therefore, one can now extract model parameters without relying on an explicit form of parametrization, leading to a robust determination by such a model–data fit.
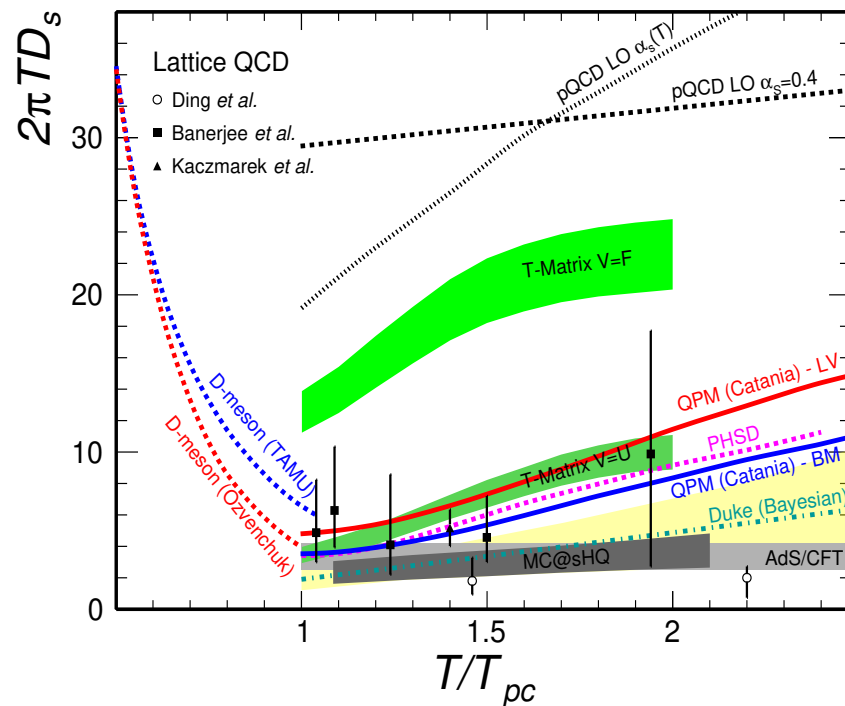
Figure 1. Spatial diffusion coefficient ($2\pi T D_s$) of charm quark in the quark–gluon plasma calculated by different approaches versus the reduced temperature (T/T_{pc}). The lattice QCD calculations in the quenched approximation [157–159] are compared with the estimations based on different models [22,40,43,92,102,160–164]. The figure is from [66].

3. Production of Heavy-Flavour Jets in Heavy-Ion Collisions

3.1. Nuclear Modification Factors of Production Yields

To address the nuclear effect in relativistic heavy-ion collisions, the nuclear modification factor R_{AA} is conventionally utilized to quantify the yield suppression of hadron/jet in A+A collisions per binary nucleon–nucleon collision relative to p+p [168],

$$R_{AA} = \frac{1}{\left\langle N_{\text{bin}}^{\text{AA}} \right\rangle} \frac{d\sigma^{\text{AA}}/\text{dydp}_\text{T}}{d\sigma^{\text{PP}}/\text{dydp}_\text{T}} \tag{13}$$

where the scaling factor $\left\langle N_{\text{bin}}^{\text{AA}} \right\rangle$ denotes the number of binary nucleon–nucleon collisions in A+A [169]. It has been observed that the values of R_{AA} of hadrons and jets are smaller than one in nucleus–nucleus collisions both at the RHIC [170–172] and LHC [173,174], and these measurements could be explained by the mechanism of partonic energy loss, which in turns serve as convincing evidence for the formation of QGP in such extremely hot and dense conditions. Meanwhile, the jet transport parameter $\hat{q} \equiv d\langle p_\perp^2 \rangle/dL$ [175] representing the strength of in-medium partonic interactions could be extracted from the available R_{AA} data by various theoretical models [167,176–179].

Additionally, to test the mass dependence of jet quenching, the R_{AA} has also been used in a comparison of the yield suppression between heavy-flavour jets and inclusive jets. Benefiting from the fact that heavy-flavour jets are produced abundantly as the centre-mass energy increases in hadronic collisions at the LHC, the exploration of a heavy quark-tagged jet produced in heavy-ion collisions has gradually attracted much attention. The first experimental effort focused on the production of a b-jet was implemented by the CMS collaboration [121] in 2013, as shown in the left plot of Figure 2, where a b-jet is defined as jets containing at least one B hadron inside the jet-cone. The red points are the CMS data and the coloured bands are the theoretical calculations. This measurement accounts for the b-jet samples in minimum bias collisions (0–100%). We note that even with large experimental uncertainties, the b-jet R_{AA} slightly increases with jet p_T and varies from 0.4 to

0.8. Significant suppression of the b-jet yield in Pb+Pb collisions at $\sqrt{s_{NN}}$ = 2.76 TeV relative to the p+p baseline was observed for the first time, which indicates that bottom quarks strongly interact with the hot/dense nuclear matter. Furthermore, within experiment uncertainties, the results were found to be consistent with the pQCD-based calculations conducted in [180] when the coupling factor g^{med} varied from 1.8 to 2.2.
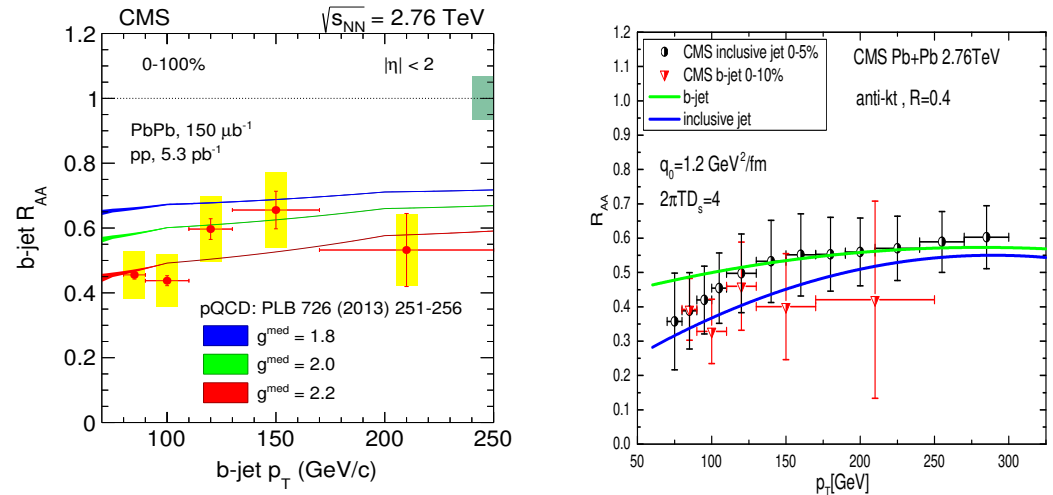

Figure 2. Left: the measured nuclear modification factor R_{AA} of the inclusive b-jet versus b-jet p_T by the CMS collaboration in Pb+Pb at $\sqrt{s_{NN}}$ = 2.76 TeV for minimum bias collisions [121]. **Right**: the comparison of R_{AA} between the inclusive jets and b-jets versus jet p_T in central Pb+Pb collisions at $\sqrt{s_{NN}}$ = 2.76 TeV [104]. The figures are from [104,121].

To address the difference of the yield suppression between the b-jet and inclusive jet (mainly initiated by a massless light quark or gluon), a direct comparison of their R_{AA} in the right plot of Figure 2 was presented by the SHELL approach, which applies a Langevin transport model to describe heavy quark propagation in the QGP [104] in central Pb+Pb collisions at $\sqrt{s_{NN}}$ = 2.76 TeV, as well as the next-to-leading order pQCD calculations matched with the parton shower effect for the p+p baseline [142,181]. In the model, the jet transport parameter $\hat{q}$ was extracted by the production of an identified hadron in A+A collisions [182], and then the spatial diffusion coefficient D_s of heavy quarks can be determined by the D meson R_{AA} data [26,127]. The measured R_{AA} of the inclusive jet with the centrality of 0–5% [183] and b-jet with 0–10% [121] are also illustrated in the plot of Figure 2. Although the R_{AA} of the b-jet seems to be slightly smaller than that of the inclusive jet, the CMS collaboration claims that no clear difference of R_{AA} between the inclusive jet and b-jet was found, because the current uncertainties of the b-jet data are too large. However, the theoretical calculations in [104] suggest that b-jet R_{AA} may be larger than inclusive jet R_{AA}, due to the "dead-cone" effect of the bottom quarks, which suppresses the medium-induced gluon radiation of massive heavy quarks within a cone $\theta \sim M/E$ [184]. A more precise measurement is necessary to resolve the tension between the experimental data and theoretical calculations. It is very exciting the fact that recently, the ATLAS collaboration reported preliminary results by simultaneously measuring the R_{AA} of the inclusive jet and b-jet in 0–20% Pb+Pb collisions at $\sqrt{s_{NN}}$ = 5.02 TeV [124], which shows a clear weaker suppression of the b-jet, and the features can be described by the theoretical calculations [49,104]. Although the mass hierarchy of jet quenching at the particle level has been confirmed by a lot of experimental data [185,186], it is indisputable that the ATLAS measurement makes a crucial step towards finding the mass effect at the jet level. The comparison of the c- and b-jet R_{AA} has been presented in [71] with the SCET model [187,188], which shows no significant difference at $p_T > 50$ GeV. More recently, some exploratory estimates indicate that the R_{AA} of the c-jet may be stronger than that of the inclusive jet at higher jet p_T due to their different constituents [189,190], an interesting finding to be investigated further in detail.

Beyond R_{AA}, another observation I_{AA} [16] has also been utilized to study the yield suppression of b-jets tagged by Z^0 bosons in high-energy nuclear collisions [191]. Similar to R_{AA}, I_{AA} is defined as follows,

$$I_{AA} = \frac{1}{\langle N_{\text{bin}}^{\text{AA}} \rangle} \frac{\frac{d\sigma^{\text{AA}}}{dp_T^{\text{jet}}}\big|_{p_T^{\min} < p_T^Z < p_T^{\max}}}{\frac{d\sigma^{\text{PP}}}{dp_T^{\text{jet}}}\big|_{p_T^{\min} < p_T^Z < p_T^{\max}}} \tag{14}$$

One can see that I_{AA} quantifies the yield variation of the jet in A+A collisions per binary nucleon–nucleon collision relative to the p+p baseline, after integrating the Z^0 boson p_T. It has been proposed that the associated production $Z^0 + $ b-jet may be helpful in addressing the mass dependence of the jet-quenching effect, since the $Z^0 + $ jet processes significantly exclude the contamination of gluon-initiated jets [192]. Thereby the comparison of I_{AA} between the $Z^0 + $ jet and $Z^0 + $ b-jet can provide direct features of the mass effect of heavy quark jets compared to light-quark jets. Figure 3 shows the comparisons of the calculated I_{AA} of the $Z^0 + $ b-jet and $Z^0 + $ jet in central 0–10% Pb+Pb collisions at $\sqrt{s_{NN}} = 5.02$ TeV, where the jets are reconstructed by the anti-k_T algorithm with a cone size R = 0.3 and pseudorapidity $|\eta^{\text{jet}}| < 1.6$. The calculations are presented within different p_T windows of Z^0 bosons in the three panels, namely 40–60, 60–80, and 80–100 GeV. We note that the shapes of I_{AA} are flat at the panel of $40 < p_T^Z < 60$ GeV but have downward trends at that of $80 < p_T^Z < 100$, and the I_{AA} in the right panel even shows enhancement at p_T^{jet}. This is because if one constrains the Z^0 meson momentum in the event selection, such as $80 < p_T^Z < 120$ GeV, then the selected jet distribution with p_T would fall steeper at $p_T^{\text{jet}} < 80$ GeV, which naturally leads to a relatively large value of the nuclear modification factors at $p_T^{\text{jet}} < 80$ GeV, even larger than one. Additionally, one observes that at each panel the model calculations show that I_{AA} of the $Z^0 + $ b-jet is visibly higher than that of the $Z^0 + $ jet in nucleus–nucleus collisions, which indicates that the Z^0-tagged light-quark jets lose more energy than the Z^0-tagged b-jets traversing the QGP. These comparisons would be helpful to directly test the mass effect of jet energy loss in heavy-ion collisions at the LHC from a new perspective.
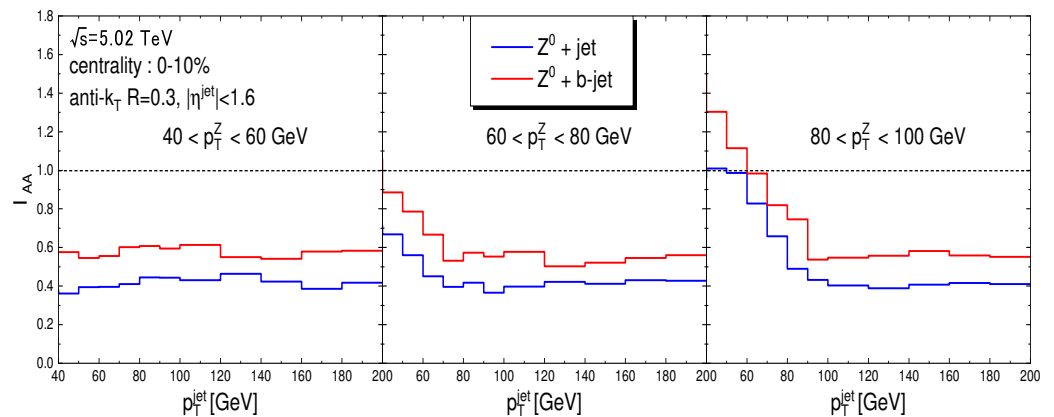

Figure 3. Nuclear modification factor I_{AA} as a function of the transverse momentum of the tagged jet within three p_T^Z windows: 40–60, 60–80, 80–120 GeV in central 0–10% Pb+Pb collisions at $\sqrt{s_{NN}} = 5.02$ TeV [191].

3.2. Transverse Momentum Imbalance

The transverse momentum imbalance ($x_J = p_{T,2}/p_{T,1}$) is another useful observation, describing the momentum asymmetry of the dijet system in the transverse plane, where $p_{T,1}$ and $p_{T,2}$ denote the leading and sub-leading jet p_T. It is noted that in the fixed-leading-order QCD calculations the two outgoing hard partons should be strictly back-to-back in the transverse ($x_J = 1$), but the higher-order corrections and vacuum shower may break the symmetry which leads to $x_J < 1$. In heavy-ion collisions, the smaller x_J of the γ+jet [193] and Z^0+jet [194] systems have been observed in Pb+Pb collisions compared to p+p, which results from the energy loss of the tagged jet. The CMS collaboration reports the measurement on x_J of the inclusive and $b\bar{b}$ dijets in Pb+Pb collisions at $\sqrt{s_{NN}}$ = 5.02 TeV [122]. In their measurements, the biggest challenge was how to select the $b\bar{b}$ dijet events initiated by the hard heavy-quark pairs, because it is crucial to address the mass effect by directly comparing such heavy-quark dijets with inclusive dijets. On the theoretical side, the production mechanisms of heavy quarks can be categorized into three classes: flavour creation (FCR), flavour excitation (FEX), and gluon splitting (GSP) [195–198], only FCR represents the dijets initiated by heavy-quark pairs originating from the hard process. The CMS collaboration suggests a strategy to separate the FCR processes by selecting $b\bar{b}$ dijets that have a large opening angle ($|\Delta\phi| > 2\pi/3$) in azimuth, which could significantly suppress the contributions of the other two. This method has also been used in theoretical studies [104,199,200]. Figure 4 shows a comparison of the averaged x_J of the inclusive and $b\bar{b}$ dijets in both p+p and Pb+Pb collisions with different centrality bins at $\sqrt{s_{NN}}$ = 5.02 TeV, as well as the experimental data [122], where $\langle x_J \rangle$ was estimated as follows.
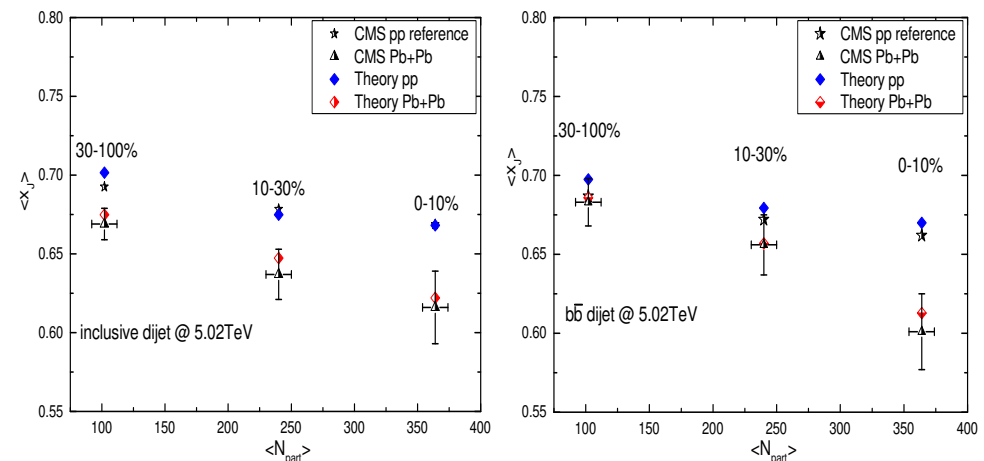

Figure 4. Averaged x_J value as a function of the number of participants calculated in p+p and Pb+Pb collisions $\sqrt{s_{NN}}$ = 5.02 TeV within different centrality bins compared with the experimental data, both for inclusive (**left**) and $b\bar{b}$ (**right**) dijets. Figures are from [104].

$$\langle x_J \rangle = \frac{1}{\sigma} \int_0^1 \frac{d\sigma}{dx_J} dx_J \qquad (15)$$

The black triangle points are the CMS data in Pb+Pb collisions, and the black star points are the p+p reference used in their measurements. The blue and red rhombus points are the theoretical calculations, while the p+p reference is provided by the Monte Carlo event generator SHERPA [142] which matches the next-to-leading order QCD matrix elements and the parton shower effect in a vacuum [201,202]. The $\langle x_J \rangle$ points of the inclusive (left panel) and $b\bar{b}$ (right panel) dijets are listed within three centrality bins which correspond to the different numbers of the participant in Pb+Pb collisions. In Figure 4, the theoretical calculations based on the SHELL model [104] show an overall decrease in $\langle x_J \rangle$ in Pb+Pb collisions relative to the p+p baseline both for the inclusive and $b\bar{b}$ dijets, consistent with the CMS data and indicates that the asymmetry between these two leading jets is amplified in A+A collisions. The reduction in $\langle x_J \rangle$ is centrality-dependent since the

in-medium interaction is sensitive to the temperature and size of the QGP. It is even more important that the calculations show that the decrease in $\langle x_J \rangle$ of the $b\bar{b}$ dijets is slightly smaller than that of the inclusive dijets within the same centrality bins. These results suggest that dijets initiated by bottom quarks may suffer smaller energy loss compared to those initiated by light quarks or gluons. Furthermore, another study on the $b\bar{b}$ dijet in heavy-ion collisions [199] proposed that the invariant mass m_{jj} of the dijet system could be a novel observation sensitive to mass effects of jet quenching.

In addition to the dijet system, the transverse momentum imbalances of the Z^0 + jet ($x_{jZ} = p_T^{\text{jet}}/p_T^Z$) and Z^0 + b-jet ($x_{bZ} = p_T^{\text{b-jet}}/p_T^Z$) have also been investigated [191]. It was found that the Z^0-tagging requirement considerably decreased the contribution of gluon-jets by 40% in Z^0 + jets compared to the dijet sample, especially at a lower jet p_T. The comparison of the medium modification on the x_J of Z^0 + jet and Z^0 + b-jet may be suitable to address the mass effect of jet quenching. Figure 5 shows the distributions of the x_{jZ} (left) and x_{bZ} (right) both in p+p and 0–10% Pb+Pb collisions at $\sqrt{s_{NN}}$ = 5.02 TeV. In the calculations, the selected Z^0 bosons are required to have $p_T^Z > 60$ GeV. The tagged jets (b-jets) are reconstructed with the anti-k_T algorithm with a cone-size R = 0.3 and pseudorapidity $|\eta^{\text{jet}}| < 1.6$, required to have $p_T^{\text{jet}} > 30$ GeV. In particular, to guarantee that the Z^0 bosons and the tagged jets are back-to-back in the transverse plane, the Z^0 + jet or Z^0 + b-jet pairs are required to have a large opening angle in azimuth, $\Delta\phi_{jZ}(\Delta\phi_{bZ}) > 7\pi/8$. The differences of x_{jZ} (x_{bZ}) distributions in p+p and Pb+Pb collisions are also shown in the lower panels. Due to the jet energy loss, the x_{jZ} and x_{bZ} distributions shift towards smaller x_J values in Pb+Pb collisions relative to p+p. Furthermore, one can find in the lower panel that the variations of x_{bZ} are slightly smaller than that of x_{jZ}. More intuitive comparisons between the averaged x_{jZ} and x_{bZ} are listed in Table 1. Within the statistical errors, the results show that $\Delta\langle x_{jz} \rangle \sim 0.136$ is considerably larger than $\Delta\langle x_{bz} \rangle \sim 0.092$, consistent with the expectation that bottom jets lose less energy than light-quark jets.
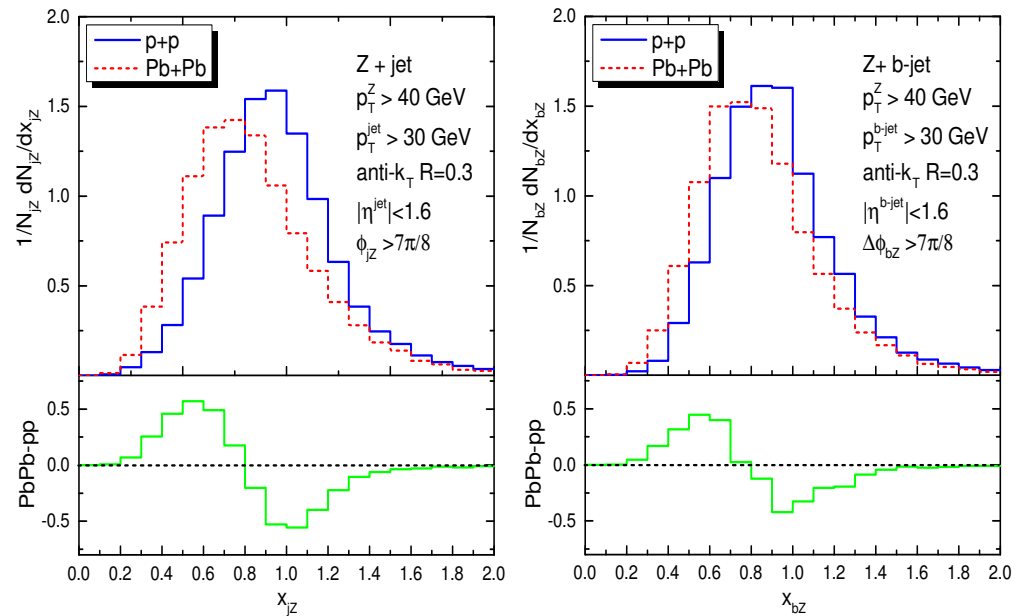

Figure 5. Distributions of x_{jZ} (x_{bZ}) of Z^0 + jet (**left**) and Z^0 + b-jet (**right**) both in p+p and 0–10% Pb+Pb collisions at $\sqrt{s_{NN}}$ = 5.02 TeV. The differences of x_{jZ} (x_{bZ}) distributions in p+p and Pb+Pb collisions (green line) are also shown in the lower panels. Figures are from Ref. [191].

Table 1. The averaged x_J of Z^0 + jet and Z^0 + b-jet both in p+p and Pb+Pb collisions at $\sqrt{s_{NN}}$ = 5.02 TeV, as well as their variations $\Delta x_J = \langle x_J \rangle_{\text{pp}} - \langle x_J \rangle_{\text{PbPb}}$. The statistical errors of x_J in the simulations are also presented. Table is from Ref. [191].

	Z^0 + jet	Z^0 + b-jet
$\langle x_J \rangle_{pp}$	0.987 ± 0.0047	0.941 ± 0.0056
$\langle x_J \rangle_{PbPb}$	0.851 ± 0.0061	0.849 ± 0.0064
$\Delta \langle x_J \rangle$	0.136 ± 0.0108	0.092 ± 0.012

3.3. Angular Correlation

Jet angular correlations, such as $\Delta \phi$ distribution of dijets [203,204] and γ/Z^0 + jet [205,206], are useful observable to address the medium-induced transverse momentum effect. In this context, estimating the medium modification on the angular distribution of heavy quark dijets in nucleus–nucleus collisions may also be of interest from the theoretical point of view. As shown in the left plot of Figure 6, medium modification of the azimuthal angular correlations ($\Delta \phi = |\phi_{b1} - \phi_{b2}|$) of the $b\bar{b}$ dijet system in Pb+Pb collisions with different centralities at $\sqrt{s_{NN}}$ = 5.02 TeV are calculated [207]. One can observe suppression at $\Delta \phi \sim 0$ and enhancement at $\Delta \phi \sim \pi$ in Pb+Pb collisions compared to the p+p, and the modifications are centrality dependent. Since the distributions are self-normalized, it implies that $b\bar{b}$ dijets with a larger opening angle (back-to-back) suffer relatively weaker yield suppression compared to that with a smaller one (collinear). It can be noted that the main contribution of $b\bar{b}$ dijet production at smaller $\Delta \phi$ is from the GSP process while larger $\Delta \phi_{bb}$ from the FCR process. The two b-jets from the former process share the energy of the gluon and then usually have lower p_T than that from the latter process. As a result, the yield at the smaller $\Delta \phi$ region is more sensitive to the selection cut $p_T^{\text{jet}} > 20$ GeV. Actually, in another study on the angular correlations of Z^0 + b-jet [191], it's found that initial average b-jet p_T distribution versus $\Delta \phi$ play a critical role, as shown in the right plot of Figure 6. We see that the ratio of PbPb/pp in the middle panel is flat, and the average b-jet p_T distribution is also flat. It's reasonable to guess that in Pb+Pb the azimuthal angle between b-jet and Z^0 has not been modified compared to p+p, and the overall suppression occurs at whole $\Delta \phi_{\text{bZ}}$ region. Of course, we can imagine that it is more difficult for high-p_T (>30 GeV) jets to be significantly deflected by the scattering with thermal parton.
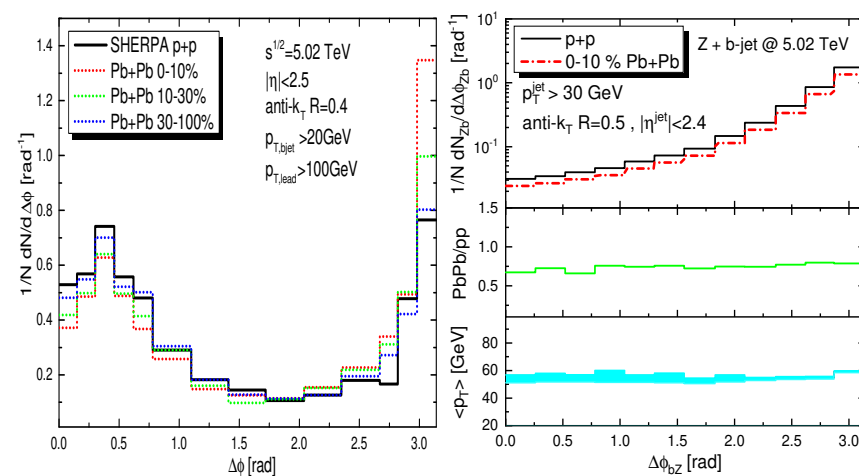

Figure 6. Left: normalized azimuthal angular distributions of $b\bar{b}$ dijet system in p+p and Pb+Pb collisions at $\sqrt{s_{NN}}$ = 5.02 TeV. Results for different centrality bins, 0–10%, 10–30%, 30–100%, are presented. **Right**: the azimuthal angular distribution of Z^0 + b-jet in p+p and 0–10% Pb+Pb collisions at $\sqrt{s_{NN}}$ = 5.02 TeV in the upper panel, while the ratio of PbPb/pp (green solid line) was shown in the middle panel and the averaged b-jet p_T (blue band) in the lower panel. Figures are from Refs. [191,207].

To probe the angular deflection caused by the in-medium p_T-broadening, observables accessible to lower p_T region are needed. For this reason, it's proposed in Ref. [105] that the heavy-flavour meson tagged by direct photon (γ+HF) may provide a promising channel, with several advantages: (1) the transverse momentum resolution of D^0 meson can be low down to ~1 GeV [127] where the angular deflection is significant, (2) the photon gauges the initial momentum of heavy quarks, therefore, it's easy to quantify the direction change, (3) the selection bias effect can be suppressed by constraining the photon energy to citeCunqueiro:2021wls. In this way, the considerable angular de-correlations between the heavy quarks and photons are predicted both in central Au+Au collisions at the RHIC and Pb+Pb collisions at the LHC. Furthermore, by constructing the 2-dimensional ($\Delta\phi, x_J$) correlation diagram of γ+HF, it's argued that the two aspects of jet quenching, energy loss, and p_T-broadening, can be well displayed simultaneously. Additionally, it's noted that another measurement on the angular correlations of D^0+hadron in Au+Au collisions at $\sqrt{s_{NN}}$ = 200 GeV may reflect the medium modification of the charm+jet correlation in the $\eta - \phi$ plane [208], that awaits further detailed investigations.

3.4. Radial Profile

The radial profile of the heavy-flavour jet represents the distribution of the angular distance $r = \sqrt{(\phi_Q - \phi_{\text{jet}})^2 + (\eta_Q - \eta_{\text{jet}})^2}$ between the heavy-flavour meson and the jet-axis in the $\eta - \phi$ plane. Systematic studies with a focus on the radial profiles of D-jet and B-jet in heavy-ion collisions are performed in Refs. [103,209]. As shown in the left panel of Figure 7, the model calculated radial profiles of D-jets both in p+p and 0–100% Pb+Pb collisions at $\sqrt{s_{NN}} = 5.02$ TeV compared to the CMS measurements [123]. The black and red triangle points represent the measured data. The D-jets are reconstructed with anti-k_T algorithm with R = 0.3 and $|\eta^{\text{jet}}| < 1.6$. All selected D-jets must satisfy $p_T^{\text{jet}} > 60$ GeV and contain at least one D^0 meson in jet-cone with $4 < p_T^D < 20$ GeV. The blue solid line is the p+p baseline provided by SHERPA [142], and the red dashed line denotes the calculations based on the SHELL model. One can observe that the model calculations show the radial profile of D-jets in Pb+Pb collisions shifts towards larger radii relative to that of p+p, which is consistent with the diffusion trend observed by the CMS collaboration. These results show a clear physics picture, that charm quarks change their moving direction when scattering with the thermal partons in the hot and dense QCD matter. The studies argue that the diffusion behavior of D meson is closely related to the p_T-broadening when charm quarks scatter with the thermal partons in the medium. It should be noted that in such an estimate the jets are required to have $p_T > 60$ GeV while D meson $p_T < 20$ GeV, which makes that the higher p_T jets can be viewed as a reference to probe the moving direction changes of charm quarks. It is found that the angular deviation $\Delta r = \sqrt{(\phi_c^f - \phi_c^i)^2 + (\eta_c^f - \eta_c^i)^2}$ of charm quarks from their initial position in the $\eta - \phi$ plane is p_T dependent, as shown in the right plot of Figure 7. The charm quarks with lower p_T are more likely to change their traveling direction via the in-medium scattering, and this feature also explains why no visible modification is observed in the CMS data for $p_T^D > 20$ GeV [123]. The angular deviation at lower p_T (<5 GeV) is dominated by elastic scattering, whereas at higher p_T by inelastic reactions. These investigations may cast light on the in-medium energy loss mechanisms and constrain the transport coefficients of heavy quarks from a new perspective. We notice that a preliminary result of the D-jet radial profile in Au+Au collisions at $\sqrt{s_{NN}} = 200$ GeV has been reported by the STAR collaboration in Ref. [125]. This result shows a similar diffusion effect of charm quark in jets in mid-central 10–40% collisions.

To test the mass effect reflected in the radial profile, an additional comparison of the medium modification between D-jet and B-jet has been presented in Refs. [210,211], where an inverse modification pattern on the radial profile of B-jets compared to D-jets is observed. The jet quenching effect seems to narrow the jet radial profiles of B-jets while broadening those of D-jets. It's demonstrated that the selection bias effect [212] in A+A

collisions may play a pivotal role. Heavy quark jets with higher p_T have narrower initial radial distributions, and would naturally lead to narrower modifications when they fall into the lower p_T domain due to jet energy loss. This reveals the fact that the final-state modification of the jet is not only influenced by the pure medium effect, but also by the other factors, such as the initial spectra and the selection bias [5].
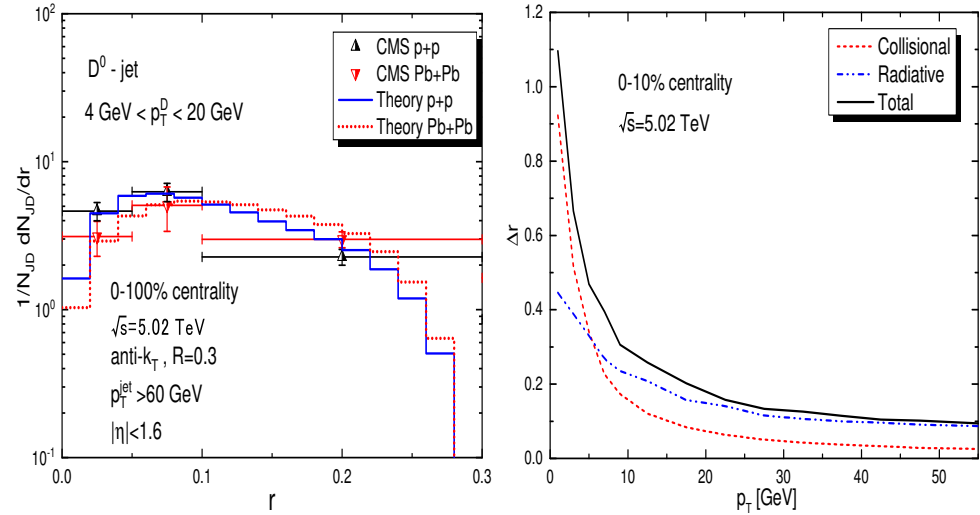

Figure 7. Left: radial profile of D-jet in p+p and Pb+Pb collisions at $\sqrt{s_{NN}}$ = 5.02 TeV. **Right**: angular deviation of charm quark as a function of initial p_T. Figures are from Refs. [103,209].

3.5. Fragmentation Function

The jet fragmentation function $D(z) = (1/N_{\text{jet}})dN_{\text{ch}}(z)/dz$ is one of the most well-explored jet substructure observable [213–215], which usually refers to the longitudinal momentum distribution of charged hadrons inside the jet-cone [216–219]. For heavy-flavour jets, the corresponding observable is the longitudinal momentum distribution of heavy-flavour mesons in jets, defined as in [112].

$$D(z_{||}) = \frac{1}{N_{\text{jet}}}\frac{dN_{\text{HQ}}(z_{||})}{dz_{||}}, \quad \text{where } z_{||} = \frac{\vec{p}_{\text{HQ}} \cdot \vec{p}_{\text{jet}}}{\vec{p}_{\text{jet}} \cdot \vec{p}_{\text{jet}}} . \tag{16}$$

On the one hand, the $D(z_{||})$ distribution may provide useful information to reveal the production mechanisms and substructure of heavy quark jets [220]. On the other hand, since $z_{||}$ denotes the momentum projection of the heavy-flavour hadron on the jet axis, the medium modification of the $D(z_{||})$ distribution in nucleus–nucleus collisions is closely related to the interplay of the partonic energy loss between the massive heavy quarks and the massless light partons [221]. Figure 8 shows the first theoretical investigation of the medium modification on the $D(z_{||})$ distributions of both D-jets and B-jets in Pb+Pb collisions at $\sqrt{s_{NN}}$ = 5.02 TeV. In these calculations, two jet p_T ranges are chosen, $5 < p_T^{\text{jet}} < 15$ GeV and $15 < p_T^{\text{jet}} < 50$ GeV. Respectively the selected D^0 (B^0) mesons are also required to have $p_{T,D^0(B^0)} > 2$ GeV and $p_{T,D^0(B^0)} > 5$ GeV. The black solid lines represent the p+p baseline of $D(z_{||})$ distributions calculated by the POWHEG+PYTHIA8 event generator [141,222–224], and the orange dash lines are the theoretical calculations in Pb+Pb collisions based on the SHELL model. The upper and middle panels correspond to the $D(z_{||})$ distributions of *D*-jets and *B*-jets, while the lower panels are their nuclear modification $D(z_{||})_{PbPb}/D(z_{||})_{pp}$ (green is D-jet and yellow B-jet). One can observe that the initial $D(z_{||})$ distributions in p+p are sensitive to the kinematic region of jet and heavy-flavour hadron, especially for D-jets. Moreover, even within the same kinematic region, a B-jet has an evident harder fragmentation pattern compared to a D-jet. The difference could be relevant to the fact that the stronger "dead-cone" effect suffered in heavier bottom quarks, in other words, the bottom quarks radiate less gluon and carry more energy fraction of jets

than charm quarks. Besides, the contribution of the GSP process may also play different roles in the production of B-jets and D-jets, which may lead to additional differences in their $z_{||}$ distributions [221]. In nuclear collisions, the main finding is that the jet quenching effect results in softer fragmentation patterns of heavy-flavour jets in the QGP compared to that in a vacuum. It's different from what one could naively argue, that is, the energy fraction of heavy quarks in jets may increase because heavy quarks lose less energy than light partons. The modification of $D(z_{||})$ reveals the different energy loss mechanisms between the single parton and the full jet. Critically, the lost energy from the jet constituents may be partially brought back to the jet energy by the reconstruction procedures. This is an essential difference in energy loss mechanisms between the full-jet and the single parton, which leads to less energy loss of full-jet compared to heavy quarks. Therefore, stronger medium modification of $D(z_{||})$ can be obtained with larger R, which may be related to the R-dependence of jet energy loss [225,226]. Furthermore, stronger medium modification of $D(z_{||})$ is observed for B-jets compared to D-jets, due to their different initial spectra.
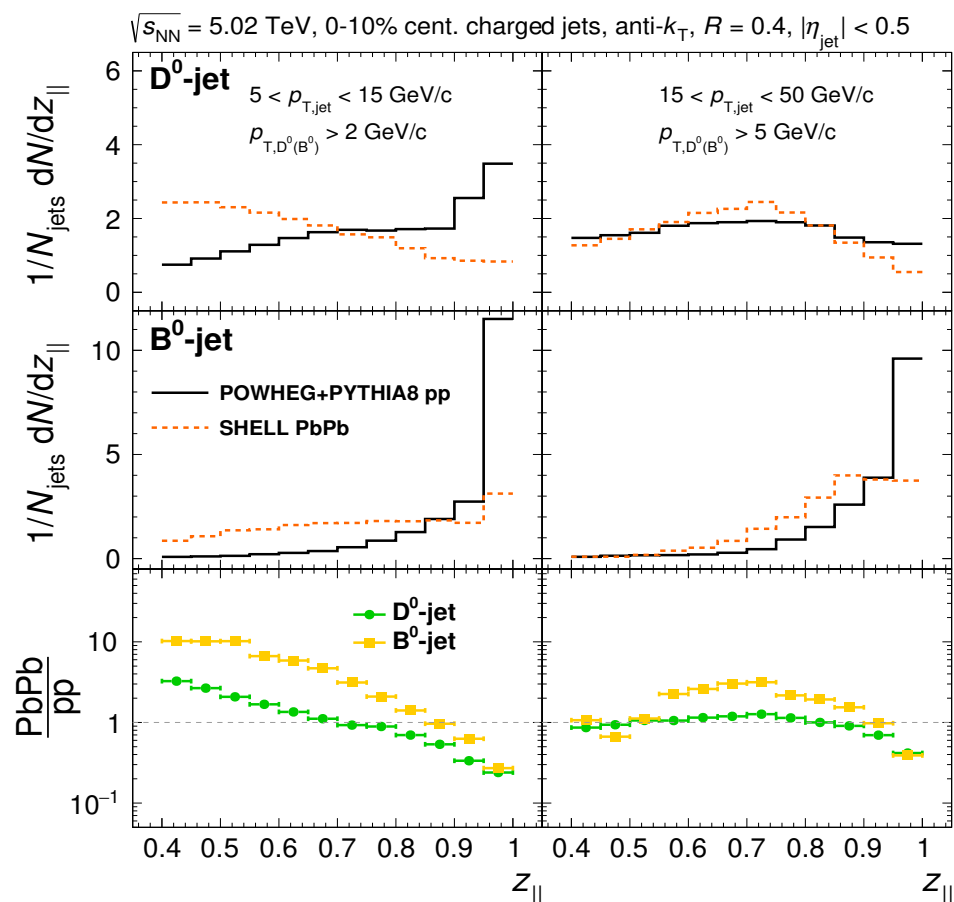

Figure 8. $D(z_{||})$ distributions of D-jet and B-jet within two p_T windows both in p+p and 0–10% Pb+Pb collisions, as well as the medium modifications (PbPb/pp). Figure is from Ref. [221].

3.6. The "Dead-Cone" Effect and Other Observables

Until now, there are a few other heavy-flavour jet observables accessible in the current experimental measurements at the LHC, which have also attracted attention from the high-energy nuclear physics community. We briefly discuss them in the following.

- The Cambridge-Aachen (CA) declustering techniques [227] which can help to obtain the angular-ordered pairwise tree of subjets [228] and the Soft Drop condition mentioned above enable us to expose the most basic heavy quark splitting structure by measuring the splitting-angle distributions in D^0 meson jets in p+p collisions at $\sqrt{s_{NN}} = 13$ TeV [229]. It has been measured in three different energy intervals of the radiators: $5 \leq E_{Radiator} \leq 10$ GeV, $10 \leq E_{Radiator} \leq 20$ GeV and

$20 \leq E_{\text{Radiator}} \leq 30$ GeV and constrain the transverse momentum of the D^0 meson in jet to be $2 < p_T^{D^0} < 36$ GeV/c. The ALICE collaboration directly observed for the first time a clear distribution suppression at the splitting angle smaller than the ratio of quark mass and the energy of such quark radiator: $\theta \leq M_{\text{charm}}/E_{\text{radiator}}$, known as the "dead-cone" effect [230,231]. Such a heavy quark jet and its substructure measurement reveal and confirm this most basic property of a fast quark interacting with the vacuum described by the QCD theory.

A subsequent phenomenology study exposed the "dead-cone" effect of the medium-induced gluon radiation of jet queching [53,150,184], by calculating the emission angle distribution of the heavy-flavour quark initiated splittings in a D^0 meson tagged jet and that of the light parton initiated splittings with the existence of the QGP in Pb+Pb collisions at $\sqrt{s_{NN}} = 5.02$ TeV [232], as demonstrated in Figure 9. Very interestingly, they find the collisional energy loss mechanism will not obscure the observation of the "dead-cone" effect in the medium-induced radiation. Such a proposal has also been verified by an analytical study that proposes a new jet substructure groomer that selects the most collinear splitting in a QCD jet above a certain transverse momentum cutoff [233]. It's also found in another study that the "dead-cone" domain would be partially filled by the medium-induced emission as heavy quarks traversing QGP [150].
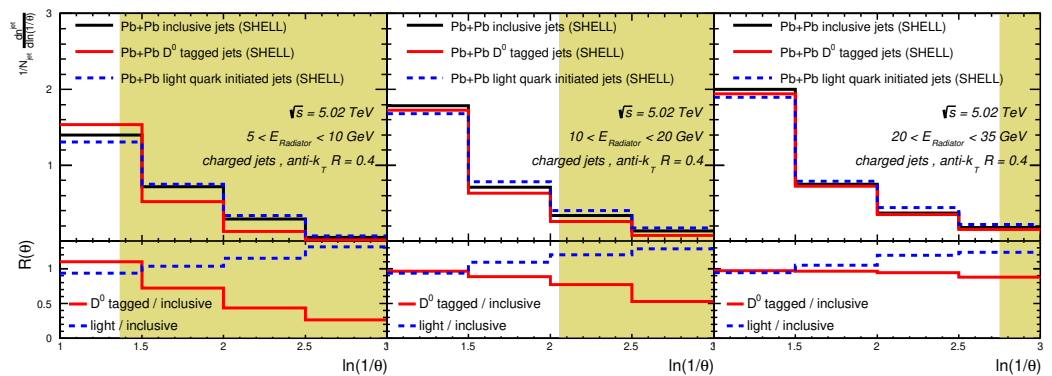

Figure 9. The splitting-angle distributions for D^0 meson tagged jets, inclusive jets and also light-quark jets normalized to the number of jets in Pb+Pb collisions at $\sqrt{s} = 5.02$ TeV (upper plots) and also the D^0 meson tagged jets/inclusive jets (light-quark jets/inclusive jets) ratios (bottom plots) calculated for three energy intervals of the radiators: $5 < E_{\text{Radiator}} < 10$ GeV (left panel), $10 < E_{\text{Radiator}} < 20$ GeV (middle panel) and $20 < E_{\text{Radiator}} < 30$ GeV (right panel). The shaded areas correspond to the angles at which the radiation is suppressed due to the "dead-cone" effect. Figure is from Ref. [232].

- The jet shape $\rho(r)$ describes the transverse energy profile of charged hadrons as a function of the angular distance from the jet axis. This observable has been well-studied for light flavor jets [205,234] to search the medium response effect as energetic parton dissipating energy to the medium [6]. The measurement of the medium modification on the b-jet shape has been reposted in Refs. [118,128] by the CMS collaboration. On the ond hand, the comparison of jet shapes of b-jets in Pb+Pb and p+p collisions shows the presence of the QGP modifies the energy distributions around the jet axis of b-jets. On the other hand, their measurements indicate a stronger jet energy redistribution of b-jets at larger radii compared to that of inclusive jets. Generally speaking, the bottom quarks are expected to dissipate less energy in nuclear collisions compared to light quarks and gluons due to the "dead-cone" effect. However, at larger jet radii, the medium response effect plays the dominant role in the enhancement of jet energy distribution in Pb+Pb collisions compared to the p+p baseline. Therefore, these interesting results may suggest that the heavier quark, like the bottom, may drive a stronger medium response effect than a massless parton. In this context, the heavy-

flavour jets can serve as promising sensitive probes to the quasi-particle excitation of the quark soup.

- The Soft Drop (SD) grooming procedures reveal the two-prong structure of a jet, described by the momentum sharing z_g and opening angle R_g [228], which establishes the connection between the final state observable to the parton splitting function. The splitting history could be helpful to identify the production mechanisms of heavy-flavour jets [235,236]. Heavy quark jets from the gluon splitting process usually tend to have more balanced z_g and larger R_g compared to that from the FEX and FCR. The first measurement of the D-jet splitting function is performed by ALICE [237], and some theoretical efforts which focus on the medium modifications of z_g and R_g of c- and b-jets are presented in Refs. [238,239]. The medium effects result in more imbalanced z_g distribution and larger opening angles between the two subjets in the heavy quark jets, similar to the medium modification of inclusive jets observed by the CMS [240] and ALICE [241] collaboration.

4. Summary and Conclusions

This review covers the current development of theoretical studies on heavy-flavour jets in ultra-relativistic heavy-ion collisions. We introduce the recent theoretical advances of heavy-flavour production in heavy-ion collisions and then give a comprehensive discussion of several recent investigations relating to the heavy-flavour jet observables.

- We briefly overview the recent theoretical advances that help us understand the heavy-flavour production in heavy-ion collisions, mainly focusing on the initial production, transport approaches, hadronization mechanism, and diffusion coefficient extraction. These phenomenological studies based on the transport models reveal a fact that the elastic scattering of heavy quarks is dominant at lower p_T region ($p_T^Q < 5m_Q$), while the inelastic one dominate the high p_T regions. Besides, different from the fragmentation hadronization of heavy quarks in a vacuum, within the hot and dense nuclear matter, the coalescence mechanism plays an important role in explaining the large collective flow and the enhancement of baryon-to-meson ratio of a charmed hadron in nucleus–nucleus collisions at the RHIC and the LHC. The diffusion coefficient of heavy quarks in the QGP has been extracted by various theoretical frameworks, which implies that $2\pi T D_s$ slightly increases with temperature. The newly developed Bayesian inference approach may be promising to implement a robust determination of the transport coefficient of heavy quarks by a model-data fit.

- The studies on yield suppression and momentum imbalance of heavy-flavour jets are dedicated to addressing the mass effect of jet energy loss. Theoretical investigations predict stronger yield suppression of light quark jets compared to heavy-flavour jets, which is preliminarily proven by the recent ATLAS measurement of b-jet R_{AA}. However, the dijet asymmetry shows a reduced sensitivity to the jet quenching effect, therefore the difference of the medium modification on x_J between inclusive and $b\bar{b}$ dijets seems to be moderate. We have to say the nuclear modification factor is still an effective and powerful observable to test the mass effect of energy loss in QGP. On the other hand, the strategy to isolate the jets initiated by heavy quarks is also crucial to address the mass effect, since GSP processes indeed have a large contribution to the production of heavy quark jets but suffer stronger suppression in nucleus–nucleus collisions.

- An observable related to angular correlation aims at the deflection of the jet axis caused by the medium-induced p_T-broadening of jet quenching. It's found that the angular deviation caused by the in-medium scattering is hard to be observed for high-p_T jets, both for $b\bar{b}$ dijets and $Z^0 + $(b-)jet. That makes sense because higher p_T jets are more difficult to be changed by the in-medium scattering with the thermal parton in QGP. Meanwhile, medium modification on the radial profiles of jets containing lower-p_T D meson can well capture the angular de-correlation of the charm quark and the jet axis. This suggests that heavy flavors may be more suitable to address the medium-induced

p_T-broadening of jet quenching since they are experimentally accessible to the low-p_T domain where the angular deviation is visible.

- The substructure observable can reveal a wealth of information about the inner configuration of heavy-flavour jets. In the vacuum case, declustering techniques provide an inventive way to reestablish the splitting history of hard partons which helps us unlock the "dead-cone" effect of charm quark in the experiment. For heavy-flavour jets, the substructure observable also provides a unique opportunity to identify their production mechanisms. Furthermore, jet substructure, such as jet shape, seems more sensitive to the induced medium excitation in nucleus–nucleus collisions than full-jet observables. Much theoretical effort should be made to address the interplay of the "dead-cone" effect of medium-induced radiation and the medium response of heavy quarks. From the current perspective, the studies of substructures of heavy-flavour jets could play an increasingly important role in high-energy nuclear physics.

- The initial jet spectra and the "selection bias" play important roles in the medium modifications of jet substructure in nuclear collisions. Normally when we focus on the mass effect of the yield or substructure modification of heavy quark jets, it is apriori to believe that bottom jets should have a weaker medium modification in heavy-ion collisions compared to charm jets under the same conditions. However, in the studies of radial profile and fragmentation function of heavy-flavour jets, it's found that b-jets have very different initial substructure compared to that of c-jets event within the same kinematic constraints, which eventually leads to stronger medium modification of b-jets at the final-state compared to c-jets. On the other hand, the "selection bias" poses a challenge to the theoretical studies that aim at the nuclear modification mechanism of heavy-flavour jets in the hot and dense QCD medium. It brings additional "modifications" to the ratio PbPb/pp of jet substructure distributions, nevertheless, these "modifications" do not exactly reflect the change of jet substructure but only the decrease of jet energy from the higher kinematic region in Pb+Pb collisions.

Author Contributions: Conceptualization, S.W. and B.-W.Z.; methodology, W.D. and B.-W.Z.; investigation, S.W. and W.D.; writing—original draft preparation, S.W. and W.D.; writing—review and editing, B.-W.Z., E.W. and X.-N.W.; supervision, B.-W.Z., E.W. and X.-N.W. All authors have read and agreed to the published version of the manuscript.

Data Availability Statement: Not applicable.

Conflicts of Interest: The authors declare no conflict of interest.

References

1. Wang, X.N.; Gyulassy, M. Gluon shadowing and jet quenching in A + A collisions at s**(1/2) = 200-GeV. *Phys. Rev. Lett.* **1992**, *68*, 1480–1483. [CrossRef] [PubMed]
2. Gyulassy, M.; Vitev, I.; Wang, X.N.; Zhang, B.W. Jet quenching and radiative energy loss in dense nuclear matter. *Quark Gluon Plasma* **2004**, *3*, 123–191.
3. Mehtar-Tani, Y.; Milhano, J.G.; Tywoniuk, K. Jet physics in heavy-ion collisions. *Int. J. Mod. Phys. A.* **2013**, *28*, 1340013. [CrossRef]
4. Qin, G.Y.; Wang, X.N. Jet quenching in high-energy heavy-ion collisions. *Int. J. Mod. Phys. E* **2015**, *24*, 1530014. [CrossRef]
5. Cunqueiro, L.; Sickles, A.M. Studying the QGP with Jets at the LHC and RHIC. *Prog. Part. Nucl. Phys.* **2022**, *124*, 103940. [CrossRef]
6. Cao, S.; Wang, X.N. Jet quenching and medium response in high-energy heavy-ion collisions: A review. *Rept. Prog. Phys.* **2021**, *84*, 024301. [CrossRef]
7. Collins, J.C.; Perry, M.J. Superdense Matter: Neutrons or Asymptotically Free Quarks? *Phys. Rev. Lett.* **1975**, *34*, 1353. [CrossRef]
8. Wang, X.N. Effect of jet quenching on high p_T hadron spectra in high-energy nuclear collisions. *Phys. Rev. C* **1998**, *58*, 2321. [CrossRef]
9. Wang, E.; Wang, X.N. Parton energy loss with detailed balance. *Phys. Rev. Lett.* **2001**, *87*, 142301. [CrossRef]

10. Majumder, A.; Wang, E.; Wang, X.N. Modified dihadron fragmentation functions in hot and nuclear matter. *Phys. Rev. Lett.* **2007**, *99*, 152301. [CrossRef]

11. Wang, E.; Wang, X.N. Jet tomography of dense and nuclear matter. *Phys. Rev. Lett.* **2002**, *89*, 162301. [CrossRef] [PubMed]

12. Zhang, H.; Owens, J.F.; Wang, E.; Wang, X.N. Dihadron tomography of high-energy nuclear collisions in NLO pQCD. *Phys. Rev. Lett.* **2007**, *98*, 212301. [CrossRef]

13. Vitev, I.; Zhang, B.W. Jet tomography of high-energy nucleus-nucleus collisions at next-to-leading order. *Phys. Rev. Lett.* **2010**, *104*, 132001. [CrossRef] [PubMed]

14. He, Y.; Pang, L.G.; Wang, X.N. Gradient Tomography of Jet Quenching in Heavy-Ion Collisions. *Phys. Rev. Lett.* **2020**, *125*, 122301. [CrossRef] [PubMed]

15. Wang, X.N.; Huang, Z.; Sarcevic, I. Jet quenching in the opposite direction of a tagged photon in high-energy heavy ion collisions. *Phys. Rev. Lett.* **1996**, *77*, 231–234. [CrossRef]

16. Neufeld, R.B.; Vitev, I.; Zhang, B.-W. The Physics of Z^0/γ^*-tagged jets at the LHC. *Phys. Rev. C* **2011**, *83*, 034902. [CrossRef]

17. Dai, W.; Vitev, I.; Zhang, B.W. Momentum imbalance of isolated photon-tagged jet production at RHIC and LHC. *Phys. Rev. Lett.* **2013**, *110*, 142001. [CrossRef]

18. Wang, X.N.; Zhu, Y. Medium Modification of γ-jets in High-energy Heavy-ion Collisions. *Phys. Rev. Lett.* **2013**, *111*, 062301. [CrossRef]

19. Li, H.; Liu, F.; Ma, G.l.; Wang, X.N.; Zhu, Y. Mach cone induced by γ-triggered jets in high-energy heavy-ion collisions. *Phys. Rev. Lett.* **2011**, *106*, 012301. [CrossRef]

20. Vitev, I.; Wicks, S.; Zhang, B.W. A Theory of jet shapes and cross-sections: From hadrons to nuclei. *JHEP* **2008**, *11*, 093. [CrossRef]

21. Caucal, P.; Soto-Ontoso, A.; Takacs, A. Dynamically groomed jet radius in heavy-ion collisions. *Phys. Rev. D* **2022**, *105*, 104046. [CrossRef]

22. Andronic, A.; Arleo, F.; Arnaldi, R.; Beraudo, A.; Bruna, E.; Caffarri, D.; Conesa del Valle, Z.; Contreras, J.G.; Dahms, T.; Dainese, A.; et al. Heavy-flavour and quarkonium production in the LHC era: From proton–proton to heavy-ion collisions. *Eur. Phys. J. C* **2016**, *76*, 107.

23. Zhang, B.W.; Ko, C.M.; Liu, W. Thermal charm production in a quark-gluon plasma in Pb-Pb collisions at s**(1/2)(NN) = 5.5-TeV. *Phys. Rev. C* **2008**, *77*, 024901. [CrossRef]

24. Adamczyk, L.; Adkins, J.K.; Agakishiev, G.; Aggarwal, M.M.; Ahammed, Z.; Alekseev, I.; Alford, J.; Anson, C.D.; Aparin, A.; Arkhipkin, D.; et al. Observation of D^0 Meson Nuclear Modifications in Au+Au Collisions at $\sqrt{s_{NN}}$ = 200 GeV. *Phys. Rev. Lett.* **2014**, *113*, 142301. [CrossRef]

25. Adam, J.; Adamova, D.; Aggarwal, M.M.; Aglieri Rinella, G.; Agnello, M.; Agrawal, N.; Ahammed, Z.; Ahn, S.U.; Aiola, S.; Akindinov, A.; et al. Transverse momentum dependence of D-meson production in Pb-Pb collisions at $\sqrt{s_{NN}}$ = 2.76 TeV. *JHEP* **2016**, *3*, 018.

26. Sirunyan, A.M.; Tumasyan, A.; Adam, W.; Ambrogi, F.; Asilar, E.; Bergauer, T.; Brandstetter, J.; Brondolin, E.; Dragicevic, M.; Erö, J.; et al. Nuclear modification factor of D^0 mesons in PbPb collisions at $\sqrt{s_{NN}}$ = 5.02 TeV. *Phys. Lett. B* **2018**, *782*, 474. [CrossRef]

27. Adare, A.; Afanasiev, S.; Aidala, C.; Ajitanand, N.N.; Akiba, Y.; Al-Bataineh, H.; Alexander, J.; Aoki, K.; Aramaki, Y.; Atomssa, E.T.; et al. J/ψ suppression at forward rapidity in Au+Au collisions at $\sqrt{s_{NN}}$ = 200 GeV. *Phys. Rev. C* **2011**, *84*, 054912. [CrossRef]

28. Adamczyk, L.; Adkins, J.K.; Agakishiev, G.; Aggarwal, M.M.; Ahammed, Z.; Alekseev, I.; Alford, J.; Anson, C.D.; Aparin, A.; Arkhipkin, D.; et al. J/ψ production at low p_T in Au + Au and Cu + Cu collisions at $\sqrt{s_{NN}}$ = 200 GeV with the STAR detector. *Phys. Rev. C* **2014**, *90*, 024906. [CrossRef]

29. Abelev, B.B.; Adam, J.; Adamova, D.; Mohan Aggarwal, M.; Aglieri Rinella, G.; Agnello, M.; Agostinelli, A.; Agrawal, N.; Ahammed, Z.; Ahmad, N.; et al. Suppression of $\Upsilon(1S)$ at forward rapidity in Pb-Pb collisions at $\sqrt{s_{NN}}$ = 2.76 TeV. *Phys. Lett. B* **2014**, *738*, 361–372. [CrossRef]

30. Abelev, B.B.; Adam, J.; Adamova, D.; Aggarwal, M.M.; Aglieri Rinella, G.; Agnello, M.; Agostinelli, A.; Agrawal, N.; Ahammed, Z.; Ahmad, N.; et al. Indications of suppression of excited Υ states in PbPb collisions at $\sqrt{s_{NN}}$ = 2.76 TeV. *Phys. Rev. Lett.* **2011**, *107*, 052302.

31. Adam, J.; Adamczyk, L.; Adams, J.R.; Adkins, J.K.; Agakishiev, G.; Aggarwal, M.M.; Ahammed, Z.; Alekseev, I.; Anderson, D.M.; Aoyama, R.; et al. First Observation of the Directed Flow of D^0 and $\overline{D^0}$ in Au+Au Collisions at $\sqrt{s_{NN}}$ = 200 GeV. *Phys. Rev. Lett.* **2019**, *123*, 162301. [CrossRef]

32. Acharya, S.; Adamova, D.; Adler, A.; Adolfsson, J.; Aggarwal, M.M.; Aglieri Rinella, G.; Agnello, M.; Agrawal, N.; Ahammed, Z.; Ahmad, S.; et al. Probing the effects of strong electromagnetic fields with charge-dependent directed flow in Pb-Pb collisions at the LHC. *Phys. Rev. Lett.* **2020**, *125*, 022301. [CrossRef]

33. Abelev, B.B.; Adam, J.; Adamova, D.; Mohan Aggarwal, M.; Aglieri Rinella, G.; Agnello, M.; Agostinelli, A.; Agrawal, N.; Ahammed, Z.; Ahmad, N.; et al. Azimuthal anisotropy of D meson production in Pb-Pb collisions at $\sqrt{s_{NN}}$ = 2.76 TeV. *Phys. Rev. C* **2014**, *90*, 034904. [CrossRef]

34. Adamczyk, L.; Adkins, J.K.; Agakishiev, G.; Aggarwal, M.M.; Ahammed, Z.; Ajitanand, N.N.; Alekseev, I.; Anderson, D.M.; Aoyama, R.; Aparin, A.; et al. Measurement of D^0 Azimuthal Anisotropy at Midrapidity in Au+Au Collisions at $\sqrt{s_{NN}}$ = 200 GeV. *Phys. Rev. Lett.* **2017**, *118*, 212301. [CrossRef] [PubMed]

35. Acharya, S.; Adamova, D.; Adolfsson, J.; Aggarwal, M.M.; Aglieri Rinella, G.; Agnello, M.; Agrawal, N.; Ahammed, Z.; Ahmad, S.; Ahmad, N.; et al. *D*-meson azimuthal anisotropy in midcentral Pb-Pb collisions at $\sqrt{s_{NN}}$ = 5.02 TeV. *Phys. Rev. Lett.* **2018**, *120*, 102301. [CrossRef] [PubMed]

36. Sirunyan, A.M.; Tumasyan, A.; Adam, W.; Ambrogi, F.; Asilar, E.; Bergauer, T.; Brandstetter, J.; Brondolin, E.; Dragicevic, M.; Erö, J.; et al. Measurement of prompt D^0 meson azimuthal anisotropy in Pb-Pb collisions at $\sqrt{s_{NN}}$ = 5.02 TeV. *Phys. Rev. Lett.* **2018**, *120*, 202301. [CrossRef] [PubMed]

37. van Hees, H.; Mannarelli, M.; Greco, V.; Rapp, R. Nonperturbative heavy-quark diffusion in the quark-gluon plasma. *Phys. Rev. Lett.* **2008**, *100*, 192301. [CrossRef]

38. Caron-Huot, S.; Moore, G.D. Heavy quark diffusion in QCD and N = 4 SYM at next-to-leading order. *JHEP* **2008**, *02*, 081. [CrossRef]

39. Djordjevic, M.; Djordjevic, M. Predictions of heavy-flavor suppression at 5.1 TeV Pb + Pb collisions at the CERN Large Hadron Collider. *Phys. Rev. C* **2015**, *92*, 024918. [CrossRef]

40. He, M.; Fries, R.J.; Rapp, R. Heavy Flavor at the Large Hadron Collider in a Strong Coupling Approach. *Phys. Lett. B* **2014**, *735*, 445. [CrossRef]

41. Kang, Z.B.; Ringer, F.; Vitev, I. Effective field theory approach to open heavy flavor production in heavy-ion collisions. *JHEP* **2017**, *3*, 146. [CrossRef]

42. Svetitsky, B. Diffusion of charmed quarks in the quark-gluon plasma. *Phys. Rev. D* **1988**, *37*, 2484. [CrossRef] [PubMed]

43. Moore, G.D.; Teaney, D. How much do heavy quarks thermalize in a heavy ion collision? *Phys. Rev. C* **2005**, *71*, 064904. [CrossRef]

44. Cao, S.; Qin, G.Y.; Bass, S.A. Heavy-quark dynamics and hadronization in ultrarelativistic heavy-ion collisions: Collisional versus radiative energy loss. *Phys. Rev. C* **2013**, *88*, 044907. [CrossRef]

45. Alberico, W.M.; Beraudo, A.; De Pace, A.; Molinari, A.; Monteno, M.; Nardi, M.; Prino, F.; Sitta, M. Heavy flavors in *AA* collisions: Production, transport and final spectra. *Eur. Phys. J. C* **2018**, *73*, 2481. [CrossRef]

46. Xu, J.; Liao, J.; Gyulassy, M. Bridging Soft-Hard Transport Properties of Quark-Gluon Plasmas with CUJET3.0. *JHEP* **2016**, *2*, 169. [CrossRef]

47. Cao, S.; Luo, T.; Qin, G.Y.; Wang, X.N. Linearized Boltzmann transport model for jet propagation in the quark-gluon plasma: Heavy quark evolution. *Phys. Rev. C* **2016**, *94*, 014909. [CrossRef]

48. Das, S.K.; Plumari, S.; Chatterjee, S.; Alam, J.; Scardina, F.; Greco, V. Directed Flow of Charm Quarks as a Witness of the Initial Strong Magnetic Field in Ultra-Relativistic Heavy Ion Collisions. *Phys. Lett. B* **2017**, *768*, 260. [CrossRef]

49. Ke, W.; Xu, Y.; Bass, S.A. Linearized Boltzmann-Langevin model for heavy quark transport in hot and dense QCD matter. *Phys. Rev. C* **2018**, *98*, 064901. [CrossRef]

50. Li, S.Q.; Xing, W.J.; Liu, F.L.; Cao, S.; Qin, G.Y. Heavy flavor quenching and flow: The roles of initial condition, pre-equilibrium evolution, and in-medium interaction. *Chin. Phys. C* **2020**, *44*, 114101. [CrossRef]

51. Yan, L.; Zhuang, P.; Xu, N. Competition between J/psi suppression and regeneration in quark-gluon plasma. *Phys. Rev. Lett.* **2006**, *97*, 232301. [CrossRef] [PubMed]

52. Liu, Y.; Qu, Z.; Xu, N.; Zhuang, P. J/psi Transverse Momentum Distribution in High Energy Nuclear Collisions at RHIC. *Phys. Lett. B* **2009**, *678*, 72–76. [CrossRef]

53. Zhang, B.W.; Wang, E.; Wang, X.N. Heavy quark energy loss in nuclear medium. *Phys. Rev. Lett.* **2004**, *93*, 072301. [CrossRef] [PubMed]

54. Djordjevic, M.; Gyulassy, M. Heavy quark radiative energy loss in QCD matter. *Nucl. Phys. A* **2004**, *733*, 265–298. [CrossRef]

55. Zhang, B.W.; Wang, E.; Wang, X.N. Multiple parton scattering in nuclei: Heavy quark energy loss and modified fragmentation functions. *Nucl. Phys. A* **2005**, *757*, 493–524. [CrossRef]

56. Fan, W.; Vujanovic, G.; Bass, S.A.; Majumder, A.; Angerami, A.; Arora, R.; Cao, S.; Chen, Y.; Dai, T.; Du, L.; et al. Multi-scale evolution of charmed particles in a nuclear medium. *arXiv* **2022**, arXiv:2208.00983.

57. Liu, F.L.; Xing, W.J.; Wu, X.Y.; Qin, G.Y.; Cao, S.; Wang, X.N. QLBT: A linear Boltzmann transport model for heavy quarks in a quark-gluon plasma of quasi-particles. *Eur. Phys. J. C* **2022**, *82*, 350. [CrossRef]

58. Ding, C.; Ke, W.Y.; Pang, L.G.; Wang, X.N. Hydrodynamic description of D meson production in high-energy heavy-ion collisions. *Chin. Phys. C* **2021**, *45*, 074102. [CrossRef]

59. Cao, S.; Sun, K.J.; Li, S.Q.; Liu, S.Y.F.; Xing, W.J.; Qin, G.Y.; Ko, C.M. Charmed hadron chemistry in relativistic heavy-ion collisions. *Phys. Lett. B* **2020**, *807*, 135561. [CrossRef]

60. Plumari, S.; Minissale, V.; Das, S.K.; Coci, G.; Greco, V. Charmed Hadrons from Coalescence plus Fragmentation in relativistic nucleus-nucleus collisions at RHIC and LHC. *Eur. Phys. J. C* **2018**, *78*, 348. [CrossRef]

61. He, M.; Rapp, R. Hadronization and Charm-Hadron Ratios in Heavy-Ion Collisions. *Phys. Rev. Lett.* **2020**, *124*, 042301. [CrossRef]

62. Rapp, R.; van Hees, H. Heavy Quarks in the Quark-Gluon Plasma. *arXiv* **2009**, arXiv:0903.1096.

63. Prino, F.; Rapp, R. Open Heavy Flavor in QCD Matter and in Nuclear Collisions. *J. Phys. G* **2016**, *43*, 093002. [CrossRef]

64. Rapp, R.; Gossiaux, P.B.; Andronic, A.; Averbeck, R.; Masciocchi, S.; Beraudo, A.; Bratkovskaya, E.; Braun-Munzinger, P.; Cao, S.; Dainese, A.; et al. Extraction of Heavy-Flavor Transport Coefficients in QCD Matter. *Nucl. Phys. A* **2018**, *979*, 21–86.

65. Dong, X.; Greco, V. Heavy quark production and properties of Quark–Gluon Plasma. *Prog. Part. Nucl. Phys.* **2019**, *104*, 97. [CrossRef]

66. Dong, X.; Lee, Y.J.; Rapp, R. Open Heavy-Flavor Production in Heavy-Ion Collisions. *Ann. Rev. Nucl. Part. Sci.* **2019**, *69*, 417–445. [CrossRef]

67. Zhao, J.; Zhou, K.; Chen, S.; Zhuang, P. Heavy flavors under extreme conditions in high energy nuclear collisions. *Prog. Part. Nucl. Phys.* **2020**, *114*, 103801. [CrossRef]

68. Apolinário, L.; Lee, Y.J.; Winn, M. Heavy quarks and jets as probes of the QGP. *Prog. Part. Nucl. Phys.* **2022**, *127*, 103990. [CrossRef]

69. He, M.; van Hees, H.; Rapp, R. Heavy-Quark Diffusion in the Quark-Gluon Plasma. *arXiv* **2022**, arXiv:2204.09299.

70. Tang, Z.; Tang, Z.B.; Zha, W.; Zha, W.M.; Zhang, Y.; Zhang, Y.F. An experimental review of open heavy flavor and quarkonium production at RHIC. *Nucl. Sci. Tech.* **2020**, *31*, 81. [CrossRef]

71. Li, H.T.; Vitev, I. Inclusive heavy flavor jet production with semi-inclusive jet functions: From proton to heavy-ion collisions. *JHEP* **2019**, *7*, 148. [CrossRef]

72. Xu, J.; Liao, J.; Gyulassy, M. Consistency of Perfect Fluidity and Jet Quenching in semi-Quark-Gluon Monopole Plasmas. *Chin. Phys. Lett.* **2015**, *32*, 092501. [CrossRef]

73. Djordjevic, M. Theoretical formalism of radiative jet energy loss in a finite size dynamical QCD medium. *Phys. Rev. C* **2009**, *80*, 064909. [CrossRef]

74. Djordjevic, M.; Heinz, U.W. Radiative energy loss in a finite dynamical QCD medium. *Phys. Rev. Lett.* **2008**, *101*, 022302. [CrossRef]

75. Djordjevic, M.; Djordjevic, M. LHC jet suppression of light and heavy flavor observables. *Phys. Lett. B* **2014**, *734*, 286–289. [CrossRef]

76. Zigic, D.; Salom, I.; Auvinen, J.; Huovinen, P.; Djordjevic, M. DREENA-A framework as a QGP tomography tool. *Front. in Phys.* **2022**, *10*, 957019. [CrossRef]

77. Zigic, D.; Salom, I.; Auvinen, J.; Djordjevic, M.; Djordjevic, M. DREENA-B framework: First predictions of R_{AA} and v_2 within dynamical energy loss formalism in evolving QCD medium. *Phys. Lett. B* **2019**, *791*, 236–241. [CrossRef]

78. Zigic, D.; Salom, I.; Auvinen, J.; Djordjevic, M.; Djordjevic, M. DREENA-C framework: Joint R_{AA} and v_2 predictions and implications to QGP tomography. *J. Phys. G* **2019**, *46*, 085101. [CrossRef]

79. Wicks, S.; Horowitz, W.; Djordjevic, M.; Gyulassy, M. Heavy quark jet quenching with collisional plus radiative energy loss and path length fluctuations. *Nucl. Phys. A* **2007**, *783*, 493–496. [CrossRef]

80. Wicks, S.; Horowitz, W.; Djordjevic, M.; Gyulassy, M. Elastic, inelastic, and path length fluctuations in jet tomography. *Nucl. Phys. A* **2007**, *784*, 426–442. [CrossRef]

81. Horowitz, W.A.; Gyulassy, M. Heavy quark jet tomography of Pb + Pb at LHC: AdS/CFT drag or pQCD energy loss? *Phys. Lett. B* **2008**, *666*, 320–323. [CrossRef]

82. Horowitz, W.A. Testing pQCD and AdS/CFT Energy Loss at RHIC and LHC. *AIP Conf. Proc.* **2012**, *1441*, 889–891.

83. Uphoff, J.; Fochler, O.; Xu, Z.; Greiner, C. Heavy quark production at RHIC and LHC within a partonic transport model. *Phys. Rev. C* **2010**, *82*, 044906. [CrossRef]

84. Uphoff, J.; Fochler, O.; Xu, Z.; Greiner, C. Elliptic Flow and Energy Loss of Heavy Quarks in Ultra-Relativistic heavy Ion Collisions. *Phys. Rev. C* **2011**, *84*, 024908. [CrossRef]

85. Uphoff, J.; Senzel, F.; Xu, Z.; Greiner, C. Momentum imbalance of D mesons in ultra-relativistic heavy-ion collisions at LHC. *Phys. Rev. C* **2014**, *89*, 064906. [CrossRef]

86. Uphoff, J.; Fochler, O.; Xu, Z.; Greiner, C. Elastic and radiative heavy quark interactions in ultra-relativistic heavy-ion collisions. *J. Phys. G* **2015**, *42*, 115106. [CrossRef]

87. Gossiaux, P.B.; Aichelin, J. Towards an understanding of the RHIC single electron data. *Phys. Rev. C* **2008**, *78*, 014904. [CrossRef]

88. Gossiaux, P.B.; Bierkandt, R.; Aichelin, J. Tomography of a quark gluon plasma at RHIC and LHC energies. *Phys. Rev. C* **2009**, *79*, 044906. [CrossRef]

89. Nahrgang, M.; Aichelin, J.; Gossiaux, P.B.; Werner, K. Azimuthal correlations of heavy quarks in Pb + Pb collisions at $\sqrt{s} = 2.76$ TeV at the CERN Large Hadron Collider. *Phys. Rev. C* **2014**, *90*, 024907. [CrossRef]

90. Ke, W.; Wang, X.N. QGP modification to single inclusive jets in a calibrated transport model. *JHEP* **2021**, *05*, 041. [CrossRef]

91. Plumari, S.; Puglisi, A.; Scardina, F.; Greco, V. Shear Viscosity of a strongly interacting system: Green-Kubo vs. Chapman-Enskog and Relaxation Time Approximation. *Phys. Rev. C* **2012**, *86*, 054902. [CrossRef]

92. Das, S.K.; Scardina, F.; Plumari, S.; Greco, V. Toward a solution to the R_{AA} and v_2 puzzle for heavy quarks. *Phys. Lett. B* **2015**, *747*, 260–264. [CrossRef]

93. Plumari, S.; Alberico, W.M.; Greco, V.; Ratti, C. Recent thermodynamic results from lattice QCD analyzed within a quasi-particle model. *Phys. Rev. D* **2011**, *84*, 094004. [CrossRef]

94. Scardina, F.; Das, S.K.; Minissale, V.; Plumari, S.; Greco, V. Estimating the charm quark diffusion coefficient and thermalization time from D meson spectra at energies available at the BNL Relativistic Heavy Ion Collider and the CERN Large Hadron Collider. *Phys. Rev. C* **2017**, *96*, 044905. [CrossRef]

95. Alberico, W.M.; Beraudo, A.; De Pace, A.; Molinari, A.; Monteno, M.; Nardi, M.; Prino, F. Heavy-flavour spectra in high energy nucleus-nucleus collisions. *Eur. Phys. J. C* **2011**, *71*, 1666. [CrossRef]

96. Beraudo, A.; Pace, A.D.; Monteno, M.; Nardi, M.; Prino, F. Heavy flavors in heavy-ion collisions: Quenching, flow and correlations. *Eur. Phys. J. C* **2015**, *75*, 121. [CrossRef]

97. Cao, S.; Bass, S.A. Thermalization of charm quarks in infinite and finite QGP matter. *Phys. Rev. C* **2011**, *84*, 064902. [CrossRef]
98. Lang, T.; van Hees, H.; Steinheimer, J.; Inghirami, G.; Bleicher, M. Heavy quark transport in heavy ion collisions at energies available at the BNL Relativistic Heavy Ion Collider and at the CERN Large Hadron Collider within the UrQMD hybrid model. *Phys. Rev. C* **2016**, *93*, 014901. [CrossRef]
99. Lang, T.; van Hees, H.; Steinheimer, J.; Bleicher, M. Elliptic flow and nuclear modification factors of *D*-mesons at FAIR in a Hybrid-Langevin approach. *arXiv* **2013**, arXiv:1305.1797.
100. Lang, T.; van Hees, H.; Steinheimer, J.; Bleicher, M. Dileptons from correlated D- and D̄-meson decays in the invariant mass range of the QGP thermal radiation using the UrQMD hybrid model. *arXiv* **2013**, arXiv:1305.7377.
101. He, M.; Fries, R.J.; Rapp, R. **D_s**-Meson as Quantitative Probe of Diffusion and Hadronization in Nuclear Collisions. *Phys. Rev. Lett.* **2013**, *110*, 112301. [CrossRef]
102. He, M.; Fries, R.J.; Rapp, R. Thermal Relaxation of Charm in Hadronic Matter. *Phys. Lett. B* **2011**, *701*, 445–450. [CrossRef]
103. Wang, S.; Dai, W.; Zhang, B.W.; Wang, E. Diffusion of charm quarks in jets in high-energy heavy-ion collisions. *Eur. Phys. J. C* **2019**, *79*, 789. [CrossRef]
104. Dai, W.; Wang, S.; Zhang, B.W.; Wang, E. Transverse Momentum Balance and Angular Distribution of $b\bar{b}$ Dijets in Pb+Pb collisions. *Chin. Phys. C* **2020**, *44*, 104105. [CrossRef]
105. Wang, S.; Kang, J.W.; Dai, W.; Zhang, B.W.; Wang, E. Probing the in-medium P_T-broadening by γ+HF angular de-correlations. *Eur. Phys. J. A* **2022**, *58*, 135. [CrossRef]
106. Cassing, W.; Bratkovskaya, E.L. Parton transport and hadronization from the dynamical quasiparticle point of view. *Phys. Rev. C* **2008**, *78*, 034919. [CrossRef]
107. Cassing, W.; Bratkovskaya, E.L. Parton-Hadron-String Dynamics: An off-shell transport approach for relativistic energies. *Nucl. Phys. A* **2009**, *831*, 215–242. [CrossRef]
108. Bratkovskaya, E.L.; Cassing, W.; Konchakovski, V.P.; Linnyk, O. Parton-Hadron-String Dynamics at Relativistic Collider Energies. *Nucl. Phys. A* **2011**, *856*, 162–182. [CrossRef]
109. Adam, J.; Adamczyk, L.; Adams, J.R.; Adkins, J.K.; Agakishiev, G.; Aggarwal, M.M.; Ahammed, Z.; Alekseev, I.; Anderson, D.M.; Aoyama, R.; et al. First measurement of Λ_c baryon production in Au+Au collisions at $\sqrt{s_{NN}}$ = 200 GeV. *Phys. Rev. Lett.* **2020**, *124*, 172301. [CrossRef]
110. Vermunt, L. Measurement of Λ_c baryons and D_s^+ mesons in Pb–Pb collisions with ALICE. *Pos* **2020**, *EPS-HEP2019*, 297.
111. Sirunyan, A.M.; Tumasyan, A.; Adam, W.; Asilar, E.; Bergauer, T.; Brandstetter, J.; Brondolin, E.; Dragicevic, M.; Erö, J.; Dragicevic, M.; et al. Measurements of the charm jet cross-section and nuclear modification factor in pPb collisions at $\sqrt{s_{NN}}$ = 5.02 TeV. *Phys. Lett. B* **2017**, *772*, 306–329. [CrossRef]
112. Acharya, S.; Adamova, D.; Adler, A.; Adolfsson, J.; Aggarwal, M.M.; Aglieri Rinella, G.; Agnello, M.; Agrawal, N.; Ahammed, Z.; Ahmad, S.; et al. Measurement of the production of charm jets tagged with D^0 mesons in pp collisions at $\sqrt{s} = 7$ TeV. *JHEP* **2019**, *8*, 133.
113. Chatrchyan, S.; Khachatryan, V.; Sirunyan, A.M.; Tumasyan, A.; Adam, W.; Bergauer, T.; Dragicevic, M.; Erö, J.; Fabjan, C.; Friedl, M.; et al. Inclusive *b*-jet production in *pp* collisions at $\sqrt{s} = 7$ TeV. *JHEP* **2012**, *4*, 084.
114. Aad, G.; Abbott, B.; Abdallah, J.; Abdelalim, A.A.; Abdesselam, A.; Abdinov, O.; Abi, B.; Abolins, M.; Abramowicz, H.; Abreu, H.; et al. Measurement of $D^{*+/-}$ meson production in jets from pp collisions at sqrt(s) = 7 TeV with the ATLAS detector. *Phys. Rev. D* **2012**, *85*, 052005. [CrossRef]
115. Aad, G.; Abbott, B.K.; Abbott, D.; Abud, A.A.; Abeling, K.; Abhayasinghe, D.K.; Abidi, H.; AbouZeid, O.S.; Abramowicz, H.; Abreu, H.; et al. Measurement of *b*-quark fragmentation properties in jets using the decay $B^{\pm} \to J/\psi K^{\pm}$ in *pp* collisions at $\sqrt{s}$ = 13 TeV with the ATLAS detector. *JHEP* **2012**, *12*, 131.
116. Abelev, B.I.; Aggarwal, M.M.; Ahammed, Z.; Anderson, B.D.; Arkhipkin, D.; Averichev, G.S.; Balewski, J.; Barannikova, O.; Barnby, L.S.; Baudot, J.; et al. Measurement of D* Mesons in Jets from p+p Collisions at s**(1/2) = 200-GeV. *Phys. Rev. D* **2009**, *79*, 112006. [CrossRef]
117. Aaboud, M.; Aad, G.; Abbott, B.; Abdallah, J.; Abdinov, O.; Abeloos, B.; Aben, R.; AbouZeid, O.; Abraham, N.; Abramowicz, H.; et al. Measurement of the $b\bar{b}$ dijet cross-section in pp collisions at $\sqrt{s} = 7$ TeV with the ATLAS detector. *Eur. Phys. J. C* **2016**, *76*, 670. [CrossRef] [PubMed]
118. Sirunyan, A.M.; Tumasyan, A.; Adam, W.; Ambrogi, F.; Bergauer, T.; Dragicevic, M.; Erö, J.; Del Valle, A.E.; Flechl, M.; Fruehwirth, R.; et al. Measurement of b jet shapes in proton-proton collisions at $\sqrt{s} = 5.02$ TeV. *JHEP* **2021**, *5*, 054.
119. Khachatryan, V.; Sirunyan, A.M.; Tumasyan, A.; Adam, W.; Asilar, E.; Bergauer, T.; Brandstetter, J.; Brondolin, E.; Dragicevic, M.; Erö, J.; et al. Transverse momentum spectra of inclusive b jets in pPb collisions at $\sqrt{s_{NN}}$ = 5.02 TeV. *Phys. Lett. B* **2016**, *754*, 59. [CrossRef]
120. Acharya, S.; Adamova, D.; Adler, A.; Adolfsson, J.; Aggarwal, M.M.; Aglieri Rinella, G.; Agnello, M.; Agrawal, N.; Ahammed, Z.; Ahmad, S.; et al. Measurement of inclusive charged-particle b-jet production in pp and p-Pb collisions at $\sqrt{s_{NN}}$ = 5.02 TeV. *JHEP* **2022**, *1*, 178.
121. Chatrchyan, S.; Khachatryan, V.; Sirunyan, A.M.; Tumasyan, A.; Adam, W.; Bergauer, T.; Dragicevic, M.; Erö, J.; Fabjan, C.; Friedl, M.; et al. Evidence of b-Jet Quenching in PbPb Collisions at $\sqrt{s_{NN}}$ = 2.76 TeV. *Phys. Rev. Lett.* **2014**, *113*, 132301. [CrossRef] [PubMed]

122. Sirunyan, A.M.; Tumasyan, A.; Adam, W.; Asilar, E.; Bergauer, T.; Brandstetter, J.; Brondolin, E.; Dragicevic, M.; Erö, J.; Dragicevic, M.; et al. Comparing transverse momentum balance of b jet pairs in pp and PbPb collisions at $\sqrt{s_{NN}}$ = 5.02 TeV. *JHEP* **2018**, *3*, 181.

123. Sirunyan, A.M.; Tumasyan, A.; Adam, W.; Asilar, E.; Bergauer, T.; Brandstetter, J.; Brondolin, E.; Dragicevic, M.; Erö, J.; Dragicevic, M.; et al. Studies of charm quark diffusion inside jets using PbPb and pp collisions at $\sqrt{s_{NN}}$ = 5.02 TeV. *Phys. Rev. Lett.* **2019**, *125*, 102001. [CrossRef] [PubMed]

124. ATLAS Collaboration. Measurement of the nuclear modification factor of *b*-jets in 5.02 TeV Pb+Pb collisions with the ATLAS detector. *arXiv* **2022**, arXiv:2204.13530.

125. Roy, D. An Investigation of Charm Quark Jet Spectrum and Shape Modifications in Au+Au Collisions at $\sqrt{s_{NN}}$ = 200 GeV. *arXiv* **2022**, arXiv:2207.14434.

126. Tumasyan, A.; Adam, W.; Bergauer, T.; Dragicevic, M.; Erö, J.; Valle, A.E.D.; Fruehwirth, R.; Jeitler, M.; Krammer, N.; Lechner, L.; et al. Fragmentation of jets containing a prompt J/ψ meson in PbPb and pp collisions at $\sqrt{s_{NN}}$ = 5.02 TeV. *Phys. Lett. B* **2022**, *825*, 136842. [CrossRef]

127. Acharya, S.; Torales-Acosta, F.; Adamova, D.; Adolfsson, J.; Aggarwal, M.M.; Rinella, G.A.; Agnello, M.; Agrawal, N.; Ahammed, Z.; Ahn, S.U.; et al. Measurement of D^0, D^+, D^{*+} and D_s^+ production in Pb-Pb collisions at $\sqrt{s_{NN}}$ = 5.02 TeV. *JHEP* **2018**, *10*, 174.

128. CMS Collaboration. Search for medium effects using jets from bottom quarks in PbPb collisions at $\sqrt{s_{NN}}$ = 5.02 TeV. *arXiv* **2022**, arXiv:2210.08547.

129. Cacciari, M.; Nason, P.; Vogt, R. QCD predictions for charm and bottom production at RHIC. *Phys. Rev. Lett.* **2005**, *95*, 122001. [CrossRef]

130. Eskola, K.J.; Paukkunen, H.; Salgado, C.A. EPS09: A New Generation of NLO and LO Nuclear Parton Distribution Functions. *JHEP* **2009**, *4*, 065. [CrossRef]

131. Eskola, K.J.; Paakkinen, P.; Paukkunen, H.; Salgado, C.A. EPPS16: Nuclear parton distributions with LHC data. *Eur. Phys. J. C* **2017**, *77*, 163. [CrossRef] [PubMed]

132. Ball, R.D.; Bertone, V.; Carrazza, S.; Deans, C.S.; Debbio, L.D.; Forte, S.; Guffanti, A.; Hartland, N.P.; Latorre, J.I.; Rojo, J.; et al. Parton distributions for the LHC Run II. *JHEP* **2015**, *4*, 040. [CrossRef]

133. Peterson, C.; Schlatter, D.; Schmitt, I.; Zerwas, P.M. Scaling Violations in Inclusive e+ e- Annihilation Spectra. *Phys. Rev. D* **1983**, *27*, 105. [CrossRef]

134. Andersson, B.; Gustafson, G.; Ingelman, G.; Sjostrand, T. Parton Fragmentation and String Dynamics. *Phys. Rept.* **1983**, *97*, 31–145. [CrossRef]

135. Aversa, F.; Chiappetta, P.; Greco, M.; Guillet, J.P. QCD Corrections to Parton-Parton Scattering Processes. *Nucl. Phys. B* **1989**, *327*, 105. [CrossRef]

136. Kniehl, B.A.; Kramer, G.; Schienbein, I.; Spiesberger, H. Inclusive D^{*+-} production in p anti-p collisions with massive charm quarks. *Phys. Rev. D* **2005**, *71*, 014018. [CrossRef]

137. Kniehl, B.A.; Kramer, G.; Schienbein, I.; Spiesberger, H. Collinear subtractions in hadroproduction of heavy quarks. *Eur. Phys. J. C* **2005**, *41*, 199–212. [CrossRef]

138. Cacciari, M.; Frixione, S.; Houdeau, N.; Mangano, M.L.; Nason, P.; Ridolfi, G. Theoretical predictions for charm and bottom production at the LHC. *JHEP* **2012**, *1210*, 137. [CrossRef]

139. Sjostrand, T.; Mrenna, S.; Skands, P.Z. PYTHIA 6.4 Physics and Manual. *JHEP* **2006**, *05*, 026. [CrossRef]

140. Corcella, G.; Knowles, I.G.; Marchesini, G.; Moretti, S.; Odagiri, K.; Richardson, P.; Seymour, M.H.; Webber, B.R. HERWIG 6: An Event generator for hadron emission reactions with interfering gluons (including supersymmetric processes. *JHEP* **2001**, *01*, 010. [CrossRef]

141. Frixione, S.; Nason, P.; Oleari, C. Matching NLO QCD computations with Parton Shower simulations: The POWHEG method. *JHEP* **2007**, *11*, 070. [CrossRef]

142. Gleisberg, T.; Hoeche, S.; Krauss, F.; Schonherr, M.; Schumann, S.; Siegert, F.; Winter, J. Event generation with SHERPA 1.1. *JHEP* **2009**, *2*, 007. [CrossRef]

143. Ferini, G.; Colonna, M.; Di Toro, M.; Greco, V. Scalings of Elliptic Flow for a Fluid at Finite Shear Viscosity. *Phys. Lett. B* **2009**, *670*, 325–329. [CrossRef]

144. Ruggieri, M.; Scardina, F.; Plumari, S.; Greco, V. Thermalization, Isotropization and Elliptic Flow from Nonequilibrium Initial Conditions with a Saturation Scale. *Phys. Rev. C* **2014**, *89*, 054914. [CrossRef]

145. Beraudo, A. Dynamics of heavy flavor quarks in high energy nuclear collisions. *Nucl. Phys. A* **2014**, *931*, 145–154. [CrossRef]

146. Arnold, P.B.; Moore, G.D.; Yaffe, L.G. Photon and gluon emission in relativistic plasmas. *JHEP* **2002**, *06*, 030. [CrossRef]

147. Abir, R.; Greiner, C.; Martinez, M.; Mustafa, M.G.; Uphoff, J. Soft gluon emission off a heavy quark revisited. *Phys. Rev. D* **2012**, *85*, 054012. [CrossRef]

148. Abir, R.; Jamil, U.; Mustafa, M.G.; Srivastava, D.K. Heavy quark energy loss and D-mesons in RHIC and LHC energies. *Phys. Lett. B* **2012**, *715*, 183–189. [CrossRef]

149. Zapp, K.; Ingelman, G.; Rathsman, J.; Stachel, J.; Wiedemann, U.A. A Monte Carlo Model for 'Jet Quenching'. *Eur. Phys. J. C* **2009**, *60*, 617–632. [CrossRef]

150. Armesto, N.; Salgado, C.A.; Wiedemann, U.A. Medium induced gluon radiation off massive quarks fills the dead cone. *Phys. Rev. D* **2004**, *69*, 114003. [CrossRef]

151. Das, S.K.; Scardina, F.; Plumari, S.; Greco, V. Heavy-flavor in-medium momentum evolution: Langevin versus Boltzmann approach. *Phys. Rev. C* **2014**, *90*, 044901. [CrossRef]

152. Li, S.; Wang, C.; Wan, R.; Liao, J. Probing the transport properties of Quark-Gluon Plasma via heavy-flavor Boltzmann and Langevin dynamics. *Phys. Rev. C* **2019**, *99*, 054909. [CrossRef]

153. Das, S.K.; Ruggieri, M.; Scardina, F.; Plumari, S.; Greco, V. Effect of pre-equilibrium phase on R_{AA} and v_2 of heavy quarks in heavy ion collisions. *J. Phys. G* **2017**, *44*, 095102. [CrossRef]

154. Lin, Z.W.; Di, G.T.; Ko, C.M. Charm meson scattering cross-sections by pion and rho meson. *Nucl. Phys. A* **2001**, *689*, 965–979. [CrossRef]

155. Cao, S.; Qin, G.Y.; Bass, S.A. Energy loss, hadronization and hadronic interactions of heavy flavors in relativistic heavy-ion collisions. *Phys. Rev. C* **2015**, *92*, 024907. [CrossRef]

156. Li, S.; Liao, J. Data-driven extraction of heavy quark diffusion in quark-gluon plasma. *Eur. Phys. J. C* **2020**, *80*, 671. [CrossRef]

157. Ding, H.T.; Karsch, F.; Mukherjee, S. Thermodynamics of strong-interaction matter from Lattice QCD. *Int. J. Mod. Phys. E* **2015**, *24*, 1530007. [CrossRef]

158. Banerjee, D.; Datta, S.; Gavai, R.; Majumdar, P. Heavy Quark Momentum Diffusion Coefficient from Lattice QCD. *Phys. Rev. D* **2012**, *85*, 014510. [CrossRef]

159. Kaczmarek, O. Continuum estimate of the heavy quark momentum diffusion coefficient κ. *Nucl. Phys. A* **2014**, *931*, 633–637. [CrossRef]

160. van Hees, H.; Rapp, R. Thermalization of heavy quarks in the quark-gluon plasma. *Phys. Rev. C* **2005**, *71*, 034907. [CrossRef]

161. Song, T.; Berrehrah, H.; Cabrera, D.; Torres-Rincon, J.M.; Tolos, L.; Cassing, W.; Bratkovskaya, E. Tomography of the Quark-Gluon-Plasma by Charm Quarks. *Phys. Rev. C* **2015**, *92*, 014910. [CrossRef]

162. Horowitz, W.A. Fluctuating heavy quark energy loss in a strongly coupled quark-gluon plasma. *Phys. Rev. D* **2015**, *91*, 085019. [CrossRef]

163. Xu, Y.; Bernhard, J.E.; Bass, S.A.; Nahrgang, M.; Cao, S. Data-driven analysis for the temperature and momentum dependence of the heavy-quark diffusion coefficient in relativistic heavy-ion collisions. *Phys. Rev. C* **2018**, *97*, 014907. [CrossRef]

164. Tolos, L.; Torres-Rincon, J.M. D-meson propagation in hot dense matter. *Phys. Rev. D* **2013**, *88*, 074019. [CrossRef]

165. Bialek, W.; Callan, C.G.; Strong, S.P. Field theories for learning probability distributions. *Phys. Rev. Lett.* **1996**, *77*, 4693–4697. [CrossRef]

166. Lemm, J.C. Bayesian field theory: Nonparametric approaches to density estimation, regression, classification, and inverse quantum problems. *arXiv* **1999**, arXiv:991205.

167. Xie, M.; Ke, W.; Zhang, H.; Wang, X.N. Global constraint on the jet transport coefficient from single hadron, dihadron and γ-hadron spectra in high-energy heavy-ion collisions. *arXiv* **2022**, arXiv:2208.14419.

168. Adam, J.; Adamczyk, L.; Adams, J.R.; Adkins, J.K.; Agakishiev, G.; Aggarwal, M.M.; Ahammed, Z.; Alekseev, I.; Anderson, D.M.; Aoyama, R.; et al. Evidence from d + Au measurements for final state suppression of high p(T) hadrons in Au+Au collisions at RHIC. *Phys. Rev. Lett.* **2003**, *91*, 072304. [CrossRef]

169. Miller, M.L.; Reygers, K.S.; Sanders, J.; Steinberg, P. Glauber modeling in high energy nuclear collisions. *Ann. Rev. Nucl. Part. Sci.* **2007**, *57*, 205–243. [CrossRef]

170. Adam, J.; Adamczyk, L.; Adams, J.R.; Adkins, J.K.; Agakishiev, G.; Aggarwal, M.M.; Ahammed, Z.; Alekseev, I.; Anderson, D.M.; Aoyama, R.; et al. Particle type dependence of azimuthal anisotropy and nuclear modification of particle production in Au + Au collisions at s(NN)**(1/2) = 200-GeV. *Phys. Rev. Lett.* **2004**, *92*, 052302. [CrossRef]

171. Adare, A.; Afanasiev, S.; Aidala, C.; Ajitanand, N.N.; Akiba, Y.; Al-Bataineh, H.; Alexander, J.; Al-Jamel, A.; Angerami, A.; Aoki, K.; et al. Nuclear modification factors of ϕ mesons in d+Au, Cu+Cu and Au+Au collisions at sqrt(S_NN) = 200 GeV. *Phys. Rev. C* **2011**, *83*, 024909. [CrossRef]

172. Adler, S.S.; Afanasiev, S.; Aidala, C.; Ajitanand, N.N.; Akiba, Y.; Alexander, J.; Amirikas, R.; Aphecetche, L.; Aronson, S.H.; Averbeck, R.; et al. Nuclear modification of electron spectra and implications for heavy quark energy loss in Au+Au collisions at s(NN)**(1/2) - 200-GeV. *Phys. Rev. Lett.* **2006**, *96*, 032301. [CrossRef] [PubMed]

173. Aad, G.; Abbott, B.; Abdallah, J.; Abdelalim, A.A.; Abdesselam, A.; Abdinov, O.; Abi, B.; Abolins, M.; Abramowicz, H.; Abreu, H.; et al. Measurements of the Nuclear Modification Factor for Jets in Pb+Pb Collisions at $\sqrt{s_{NN}} = 2.76$ TeV with the ATLAS Detector. *Phys. Rev. Lett.* **2015**, *114*, 072302. [CrossRef]

174. Aaboud, M.; Aad, G.; Abbott, B.; Abdallah, J.; Abdinov, O.; Abeloos, B.; Aben, R.; AbouZeid, O.; Abraham, N.; Abramowicz, H.; et al. Measurement of the nuclear modification factor for inclusive jets in Pb+Pb collisions at $\sqrt{s_{NN}} = 5.02$ TeV with the ATLAS detector. *Phys. Lett. B* **2019**, *790*, 108–128. [CrossRef]

175. Baier, R. Jet quenching. *Nucl. Phys. A* **2003**, *715*, 209–218. [CrossRef]

176. Burke, K.M.; Buzzatti, A.; Chang, N.; Gale, C.; Gyulassy, M.; Heinz, U.; Jeon, S.; Majumder, A.; Muller, B.; Qin, G.Y.; et al. Extracting the jet transport coefficient from jet quenching in high-energy heavy-ion collisions. *Phys. Rev. C* **2014**, *90*, 014909. [CrossRef]

177. Xie, M.; Wei, S.Y.; Qin, G.Y.; Zhang, H.Z. Extracting jet transport coefficient via single hadron and dihadron productions in high-energy heavy-ion collisions. *Eur. Phys. J. C* **2019**, *79*, 589. [CrossRef]

178. Ru, P.; Kang, Z.B.; Wang, E.; Xing, H.; Zhang, B.W. Global extraction of the jet transport coefficient in cold nuclear matter. *Phys. Rev. D* **2021**, *103*, L031901. [CrossRef]

179. Cao, S.; Chen, Y.; Coleman, J.; Mulligan, J.; Jacobs, P.M.; Soltz, R.A.; Angerami, A.; Arora, R.; Bass, S.A.; Cunqueiro, L.; et al. Determining the jet transport coefficient $\hat{q}$ from inclusive hadron suppression measurements using Bayesian parameter estimation. *Phys. Rev. C* **2021**, *104*, 024905. [CrossRef]

180. Huang, J.; Kang, Z.B.; Vitev, I. Inclusive b-jet production in heavy ion collisions at the LHC. *Phys. Lett. B* **2013**, *726*, 251. [CrossRef]

181. Frixione, S.; Webber, B.R. Matching NLO QCD computations and parton shower simulations. *JHEP* **2002**, *6*, 029. [CrossRef]

182. Ma, G.Y.; Dai, W.; Zhang, B.W.; Wang, E.K. NLO Productions of ω and K_S^0 with a global extraction of the jet transport parameter in heavy-ion collisions. *Eur. Phys. J. C* **2019**, *79*, 518. [CrossRef]

183. Khachatryan, V.; Sirunyan, A.M.; Tumasyan, A.; Adam, W.; Asilar, E.; Bergauer, T.; Brandstetter, J.; Brondolin, E.; Dragicevic, M.; Erö, J.; et al. Measurement of inclusive jet cross-sections in pp and PbPb collisions at $\sqrt{s_{NN}} = 2.76$ TeV. *Phys. Rev. C* **2017**, *96*, 015202. [CrossRef]

184. Dokshitzer, Y.L.; Kharzeev, D.E. Heavy quark colorimetry of QCD matter. *Phys. Lett. B* **2001**, *519*, 199–206. [CrossRef]

185. Acharya, U.A.; Adare, A.; Aidala, C.; Ajitanand, N.N.; Akiba, Y.; Alfred, M.; Apadula, N.; Asano, H.; Azmoun, B.; Babintsev, V.; et al. Charm- and Bottom-Quark Production in Au+Au Collisions at $\sqrt{s_{NN}} = 200$ GeV. *arXiv* **2022**, arXiv:2203.17058.

186. Abdallah, M.S.; Aboona, B.E.; Adam, J.; Adamczyk, L.; Adams, J.R.; Adkins, J.K.; Aggarwal, I.; Aggarwal, M.M.; Ahammed, Z.; Anderson, D.M.; et al. Evidence of Mass Ordering of Charm and Bottom Quark Energy Loss in Au+Au Collisions at RHIC. *arXiv* **2021**, arXiv:2111.14615.

187. Ovanesyan, G.; Vitev, I. Medium-induced parton splitting kernels from Soft Collinear Effective Theory with Glauber gluons. *Phys. Lett. B* **2012**, *706*, 371. [CrossRef]

188. Sievert, M.D.; Vitev, I. Quark branching in QCD matter to any order in opacity beyond the soft gluon emission limit. *Phys. Rev. D* **2018**, *98*, 094010. [CrossRef]

189. Ke, W.; Wang, X.N.; Fan, W.; Bass, S.A. Study of heavy-flavor jets in a transport approach. *arXiv* **2020**, arXiv:2008.07622.

190. Wang, S.; Zhang, B.W.; Wang, E. Probing the mass effect of jet quenching by heavy-flavor jet in heavy-ion collisions. 2023. *In preparation*.

191. Wang, S.; Dai, W.; Zhang, B.W.; Wang, E. Z^0 Boson Associated b-jet Production in High-Energy Nuclear Collisions. *arXiv* **2020**, arXiv:2005.07018.

192. Kartvelishvili, V.; Kvatadze, R.; Shanidze, R. On Z and Z + jet production in heavy ion collisions. *Phys. Lett. B* **1995**, *356*, 589. [CrossRef]

193. Sirunyan, A.M.; Tumasyan, A.; Adam, W.; Ambrogi, F.; Asilar, E.; Bergauer, T.; Brandstetter, J.; Brondolin, E.; Dragicevic, M.; Erö, J.; et al. Study of jet quenching with isolated-photon+jet correlations in PbPb and pp collisions at $\sqrt{s_{NN}} = 5.02$ TeV. *Phys. Lett. B* **2018**, *785*, 14–39. [CrossRef]

194. Sirunyan, A.M.; Tumasyan, A.; Adam, W.; Ambrogi, F.; Asilar, E.; Bergauer, T.; Brandstetter, J.; Brondolin, E.; Dragicevic, M.; Erö, J.; et al. Study of Jet Quenching with Z + jet Correlations in Pb-Pb and pp Collisions at $\sqrt{s_{NN}} = 5.02$ TeV. *Phys. Rev. Lett.* **2017**, *119*, 082301. [CrossRef] [PubMed]

195. Nason, P.; Dawson, S.; Ellis, R.K. The One Particle Inclusive Differential Cross-Section for Heavy Quark Production in Hadronic Collisions. *Nucl. Phys. B* **1989**, *327*, 49–92. [CrossRef]

196. Beenakker, W.; van Neerven, W.L.; Meng, R.; Schuler, G.A.; Smith, J. QCD corrections to heavy quark production in hadron hadron collisions. *Nucl. Phys. B* **1991**, *351*, 507–560. [CrossRef]

197. Mangano, M.L.; Nason, P.; Ridolfi, G. Heavy quark correlations in hadron collisions at next-to-leading order. *Nucl. Phys. B* **1992**, *373*, 295–345. [CrossRef]

198. Norrbin, E.; Sjostrand, T. Production and hadronization of heavy quarks. *Eur. Phys. J. C* **2000**, *17*, 137–161. [CrossRef]

199. Kang, Z.B.; Reiten, J.; Vitev, I.; Yoon, B. Light and heavy flavor dijets production and dijets mass modification in heavy ion collisions. *Phys. Rev. D* **2019**, *99*, 034006. [CrossRef]

200. Huang, J.; Kang, Z.B.; Vitev, I.; Xing, H. Photon-tagged and B-meson-tagged b-jet production at the LHC. *Phys. Lett. B* **2015**, *750*, 287. [CrossRef]

201. Gleisberg, T.; Hoeche, S. Comix, a new matrix element generator. *JHEP* **2008**, *12*, 039. [CrossRef]

202. Schumann, S.; Krauss, F. A Parton shower algorithm based on Catani-Seymour dipole factorisation. *JHEP* **2008**, *03*, 038. [CrossRef]

203. Mueller, A.H.; Wu, B.; Xiao, B.W.; Yuan, F. Probing Transverse Momentum Broadening in Heavy Ion Collisions. *Phys. Lett. B* **2016**, *763*, 208–212. [CrossRef]

204. Jia, J.; Wei, S.Y.; Xiao, B.W.; Yuan, F. Medium-Induced Transverse Momentum Broadening via Forward Dijet Correlations. *Phys. Rev. D* **2020**, *101*, 094008. [CrossRef]

205. Luo, T.; Cao, S.; He, Y.; Wang, X.N. Multiple jets and γ-jet correlation in high-energy heavy-ion collisions. *Phys. Lett. B* **2018**, *782*, 707–716. [CrossRef]

206. Zhang, S.L.; Luo, T.; Wang, X.N.; Zhang, B.W. Z+jet correlation with NLO-matched parton-shower and jet-medium interaction in high-energy nuclear collisions. *Phys. Rev. C* **2018**, *98*, 021901. [CrossRef]

207. Wang, S.; Dai, W.; Zhang, B.W.; Wang, E. The production of $b\bar{b}$ dijets in heavy-ion collisions at the LHC. *arXiv* **2018**, arXiv:1812.00391.

208. Adam, J.; Adamczyk, L.; Adams, J.R.; Adkins, J.K.; Agakishiev, G.; Aggarwal, M.M.; Ahammed, Z.; Alekseev, I.; Anderson, D.M.; Aoyama, R.; et al. Measurement of D^0-meson + hadron two-dimensional angular correlations in Au+Au collisions at $\sqrt{s_{NN}}$ = 200 GeV. *Phys. Rev. C* **2020**, *102*, 014905. [CrossRef]

209. Wang, S.; Dai, W.; Yan, J.; Zhang, B.W.; Wang, E. Radial distribution of charm quarks in jets in high-energy heavy-ion collisions. *Nucl. Phys. A* **2021**, *1005*, 121787. [CrossRef]

210. Wang, S.; Dai, W.; Zhang, B.W.; Wang, E. Radial profile of heavy quarks in jets in high-energy nuclear collisions. *arXiv* **2020**, arXiv:2009.13959.

211. Wang, S.; Dai, W.; Zhang, B.W.; Wang, E. Radial profile of bottom quarks in jets in high-energy nuclear collisions. *Chin. Phys. C* **2021**, *45*, 064105. [CrossRef]

212. Renk, T. Biased showers: A common conceptual framework for the interpretation of high-P_T observables in heavy-ion collisions. *Phys. Rev. C* **2013**, *88*, 054902. [CrossRef]

213. Sjostrand, T.; Bengtsson, M. The Lund Monte Carlo for Jet Fragmentation and e+ e− Physics. Jetset Version 6.3: An Update. *Comput. Phys. Commun.* **1987**, *43*, 367. [CrossRef]

214. Webber, B.R. A QCD Model for Jet Fragmentation Including Soft Gluon Interference. *Nucl. Phys. B* **1984**, *238*, 492–528. [CrossRef]

215. Procura, M.; Stewart, I.W. Quark Fragmentation within an Identified Jet. *Phys. Rev. D* **2010**, *81*, 074009. [CrossRef]

216. Chatrchyan, S.; Khachatryan, V.; Sirunyan, A.M.; Tumasyan, A.; Adam, W.; Bergauer, T.; Dragicevic, M.; Erö, J.; Fabjan, C.; Friedl, M.; et al. Measurement of Jet Fragmentation in PbPb and pp Collisions at $\sqrt{s_{NN}}$ = 2.76 TeV. *Phys. Rev. C* **2014**, *90*, 024908. [CrossRef]

217. Aad, G.; Abbott, B.; Abdallah, J.; Abdelalim, A.A.; Abdesselam, A.; Abdinov, O.; Abi, B.; Abolins, M.; Abramowicz, H.; Abreu, H.; et al. Measurement of inclusive jet charged-particle fragmentation functions in Pb+Pb collisions at $\sqrt{s_{NN}}$ = 2.76 TeV with the ATLAS detector. *Phys. Lett. B* **2014**, *739*, 320–342. [CrossRef]

218. Aaboud, M.; Aad, G.; Abbott, B.; Abdallah, J.; Abdinov, O.; Abeloos, B.; Aben, R.; AbouZeid, O.; Abraham, N.; Abramowicz, H.; et al. Measurement of jet fragmentation in Pb+Pb and *pp* collisions at $\sqrt{s_{NN}}$ = 2.76 TeV with the AT-LAS detector at the LHC. *Eur. Phys. J. C* **2017**, *77*, 379. [CrossRef]

219. Aaboud, M.; Aad, G.; Abbott, B.; Abdallah, J.; Abdinov, O.; Abeloos, B.; Aben, R.; AbouZeid, O.; Abraham, N.; Abramowicz, H.; et al. Comparison of Fragmentation Functions for Jets Dominated by Light Quarks and Gluons from *pp* and Pb+Pb Collisions in ATLAS. *Phys. Rev. Lett.* **2019**, *123*, 042001.

220. ALICE Collaboration. Measurement of the production of charm jets tagged with D^0 mesons in pp collisions at $\sqrt{s}$ = 5.02 and 13 TeV. *arXiv* **2022**, arXiv:2204.10167.

221. Li, Y.; Wang, S.; Zhang, B.W. Longitudinal momentum fraction of D^0 in jets in high-energy nuclear collisions. *arXiv* **2022**, arXiv:2209.00548.

222. Nason, P. A New method for combining NLO QCD with shower Monte Carlo algorithms. *JHEP* **2004**, *11*, 040. [CrossRef]

223. Alioli, S.; Nason, P.; Oleari, C.; Re, E. A general framework for implementing NLO calculations in shower Monte Carlo programs: The POWHEG BOX. *JHEP* **2010**, *06*, 043. [CrossRef]

224. Sjostrand, T.; Mrenna, S.; Skands, P.Z. A Brief Introduction to PYTHIA 8.1. *Comput. Phys. Commun.* **2008**, *178*, 852–867. [CrossRef]

225. Aad, G.; Abbott, B.; Abdallah, J.; Abdelalim, A.A.; Abdesselam, A.; Abdinov, O.; Abi, B.; Abolins, M.; Abramowicz, H.; Abreu, H.; et al. Measurement of the jet radius and transverse momentum dependence of inclusive jet suppression in lead-lead collisions at $\sqrt{s_{NN}}$ = 2.76 TeV with the ATLAS detector. *Phys. Lett. B* **2013**, *719*, 220–241. [CrossRef]

226. Bossi, H. *R*-dependence of inclusive jet suppression and groomed jet splittings in heavy-ion collisions with ALICE. *arXiv* **2022**, arXiv:2208.14492.

227. Dokshitzer, Y.L.; Leder, G.D.; Moretti, S.; Webber, B.R. Better jet clustering algorithms. *JHEP* **1997**, *8*, 001. [CrossRef]

228. Larkoski, A.J.; Marzani, S.; Soyez, G.; Thaler, J. Soft Drop. *JHEP* **2014**, *5*, 146. [CrossRef]

229. Acharya, S.; Torales-Acosta, F.; Adamova, D.; Adolfsson, J.; Aggarwal, M.M.; Rinella, G.A.; Agnello, M.; Agrawal, N.; Ahammed, Z.; Ahn, S.U.; et al. Direct observation of the dead-cone effect in QCD. *Nature* **2022**, *605*, 440–446.

230. Dokshitzer, Y.L.; Khoze, V.A.; Troian, S.I. On specific QCD properties of heavy quark fragmentation ('dead cone'). *J. Phys. G* **1991**, *17*, 1602–1604. [CrossRef]

231. Cunqueiro, L.; Płoskoń, M. Searching for the dead cone effects with iterative declustering of heavy-flavor jets. *Phys. Rev. D* **2019**, *99*, 074027. [CrossRef]

232. Dai, W.; Li, M.Z.; Zhang, B.W.; Wang, E. Exposing the dead-cone effect of jet quenching in QCD medium. *arXiv* **2022**, arXiv:2205.14668.

233. Cunqueiro, L.; Napoletano, D.; Soto-Ontoso, A. Dead-cone searches in heavy-ion collisions using the jet tree. *arXiv* **2022**, arXiv:2211.11789.

234. Chang, N.B.; Tachibana, Y.; Qin, G.Y. Nuclear modification of jet shape for inclusive jets and γ-jets at the LHC energies. *Phys. Lett. B* **2020**, *801*, 135181. [CrossRef]

235. Goncalves, D.; Krauss, F.; Linten, R. Distinguishing b-quark and gluon jets with a tagged b-hadron. *Phys. Rev. D* **2016**, *93*, 053013. [CrossRef]

236. Ilten, P.; Rodd, N.L.; Thaler, J.; Williams, M. Disentangling Heavy Flavor at Colliders. *Phys. Rev. D* **2017**, *96*, 054019. [CrossRef]

237. ALICE Collaboration. Measurements of groomed-jet substructure of charm jets tagged by D^0 mesons in proton-proton collisions at $\sqrt{s}$ = 13 TeV. *arXiv* **2022**, arXiv:2208.04857.

238. Zhang, Q.; Dai, W.; Zhang, B.W.; Wang, E. Substructures of heavy flavor jets in pp and Pb+Pb collisions at $\sqrt{s_{NN}}$ = 5.02 TeV. *In preparation*.

239. Li, H.T.; Vitev, I. Inverting the mass hierarchy of jet quenching effects with prompt *b*-jet substructure. *Phys. Lett. B* **2019**, *793*, 259. [CrossRef]

240. Sirunyan, A.M.; Tumasyan, A.; Adam, W.; Ambrogi, F.; Asilar, E.; Bergauer, T.; Brandstetter, J.; Brondolin, E.; Dragicevic, M.; Erö, J.; et al. Measurement of the Splitting Function in *pp* and Pb-Pb Collisions at $\sqrt{s_{NN}}$ = 5.02 TeV. *Phys. Rev. Lett.* **2018**, *120*, 142302. [CrossRef]

241. Acharya, S.; Adamova, D.; Adler, A.; Adolfsson, J.; Aggarwal, M.M.; Aglieri Rinella, G.; Agnello, M.; Agrawal, N.; Ahammed, Z.; Ahmad, S.; et al. Exploration of jet substructure using iterative declustering in pp and Pb–Pb collisions at LHC energies. *Phys. Lett. B* **2020**, *802*, 135227. [CrossRef]